Doctoral Dissertation

In-situ scanning electron microscopy observation of electrode-electrolyte interfaces in an electrochemical cell

HE GADA

Supervisor: Tomitori Masahiko

Graduate School of Advanced Science and Technology

Japan Advanced Institute of Science and Technology

[Materials Science]

March 2022

Acknowledgement

I hereby express my profound gratitude and appreciation to my supervisor professor Tomitori Masahiko for his extraordinary patient guidance in research work and generous financial support during my PhD. His constant encouragement and mental support always keep me in the right track toward the final goal. Being a member of his group is one of the most fortunate things in my entire life. Without his tremendous effort, it was impossible for me to complete the project on my own. He is more a mentor than a teacher; I will always be deeply grateful.

I would like to thank my minor research supervisor professor Matsumi Noriyoshi for giving me a chance to conduct my Sub-thesis project in his laboratory. My thanks to Assistant professor Badam Rajashekar and other members from Matsumi Laboratory for giving me enormous support during my minor research experiment.

My great thanks to my internal committee members, professor Tomitori Masahiko, Professor Oshima Yoshifumi, Professor Matsumi Noriyoshi and Associate Professor Akabori Masashi for serving as my committee members. My special thanks to Professor Arai Toyoko from Kanazawa University as an

external committee member. Your brilliant comments and suggestions made my doctoral defense to be an enjoyable journey.

Finally, I would like to express my warmest gratitude to my beloved wife, for her love, patience, and mental support during my hard PhD life in JAIST.

JAIST, Nomi, Ishikawa, Japan

He Gada March 2022

Contents

Chapter 1 Introduction

1.1 About electrochemical reaction

1.1.1 Principle of electrochemical reaction

Electrochemistry is the chemical reactions accompanying electric charge transfer between two substances-such as electrode and electrolyte. When an externally supplied bias voltage cause a chemical reaction as in electrolysis, or if a voltage difference is generated by a spontaneous chemical reaction as in a battery, it is called an electrochemical reaction. Chemical reactions where electrons are directly transferred between molecules and/or atoms are called oxidation-reduction or (redox) reactions. In general, electrochemistry describes the overall reactions when individual redox reactions are separate but connected by an external electric circuit and an intervening electrolyte.

Electroplating is one kind of the electric energy initiated redox reaction that it would not proceed spontaneously, for example: for an electrochemical cell that consists of copper wire electrode and copper salt electrolyte. Copper atoms from anode will change to Cu^{2+} when external supplied positive potential is applied to anode, and these Cu^{2+} are dissolved in the electrolyte.

When a negative potential is applied to cathode, the Cu^{2+} surrounding this electrode will turn into copper atoms. To make this possible Cu^{2+} are conducted through the electrolyte, while simultaneously two electrons are conducted through a wire and power source between the anode and cathode. This separation of ionic path and electrical path is the crux between traditional redox reactions and electrochemical redox reactions.

The electrochemical technique is widely applied like, electrochemical cell, corrosion protecting, electrolytic synthesis, refining of metal, biobattery and so on. Both the theoretical research and technical application become more and more important for the development of society.

The Italian physician and anatomist luigi Galvani first discovered bioelectricity in the late 18^{th} century, when studying the influence of static electricity to dead frog's body (Figure 1). Find out that, "the muscle of dead frog's leg twitched when struck by an electric spark", come to conclusion of the electric energy carried by liquid ions would cause muscle movement.

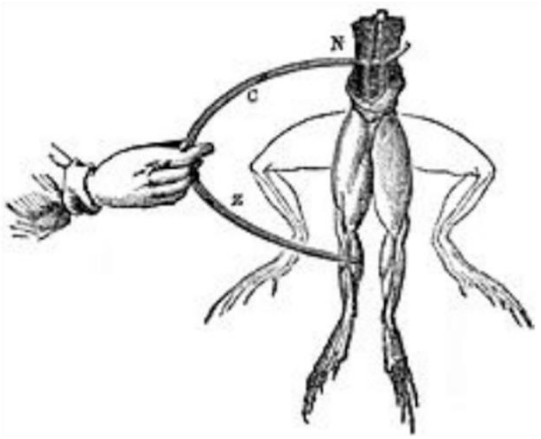

Fig. 1. The Italian physician and anatomist luigi Galvani (1737-1798) and the schematic diagram of the experiment, when electrode touch the frog leg, they would move upward.
[https://en.wikipedia.org/wiki/Luigi_Galvani]

In 1799, the Italian physicist Alessandro Volta invented the first Volta battery, discovered that electricity flew through the wire when immersing the zinc plate and silver plate in the salt water and connecting them with wire.

In 1832, the British scientist Michael Faraday discovered the law of electrochemistry during conducting electrolysis reaction experiment, and it became the fundamental principle in electrochemistry study.

In 1839, the British scientist William Robert Grove invented the first fuel cell that turn the chemical energy of oxygen hydrogen reaction into electric energy.

In 1840, Elkington from England obtained the first patent of cyanide silver plating and industrial produced, meaning the beginning of the electroplating industry.

In 1843, Ernst Werner von Siemens from Germany invented the nickel electroplating technique, it was very important for the development of printing technology.

In 1866, the German company SIEMENS first initiated the working principle of electric generator and produced first DC motor, meaning the large-scale application of electrolysis technique in industrial world.

In 1887, the Danish inventor Wilhelm Hellesen invented the first dry battery in the world.

In 1991, the Japanese company SONY commercialized the rechargeable Lithium-ion battery, and commercial production was begun in 1999 under collaboration of several companies.

1.1.2 Analysis of electrochemical reaction

Electrochemical measurements were carried out by an electrochemical cell that consists of two or three terminals, and an electrical circuit, which is used for applying or measuring the current and potential. The simplest electrochemical cell has two terminals. The electrode that transfer electron with electrolyte is called working electrode (WE). The other electrode that returning same electric current value that generated from working electrode to the system is called counter electrode (CE). Theoretically, the counter electrode's potential remains constant so that we can assign any change to the working electrode in the overall electrochemical cell potential. If the counter electrode's potential is not constant, we replace it with two electrodes: a reference electrode (RE) whose potential remains constant against potential of working electrode.

According to the Nernst equation that provides a mathematical relationship between the potential of electrode and activities of oxidized and reduced forms of analyte at the interface of electrode and electrolyte, we cannot simultaneously control the current and the potential.

It relates the potential of electrochemical cell (E) to the standard potential of a species (E0) and the relative activities of the oxidized (Ox) and reduced (Red) analyte in the system at equilibrium. In the equation, F is Faraday's constant, R

is the universal gas constant, n is the number of electrons, and T is the temperature

$$E = E^0 + \frac{RT}{nF} \ln \frac{(Ox)}{(Red)} \qquad 1.1$$

$$E = E^0 + 2.3026 \frac{RT}{nF} \log_{10} \frac{(Ox)}{(Red)} \qquad 1.2$$

If a solution of redox couple is at equilibrium, the current is zero and the potential is given by equation 1.1. If we change the potential away from its equilibrium position, current flows as the system moves toward its new equilibrium position. Although the initial current is quite large, it decreases over time reaching zero when the reaction reaches equilibrium. The current, therefore, changes in response to the applied potential. Alternatively, we can pass a controlled current through the electrochemical cell, forcing the reduction of reductant to oxidant. Because the concentrations of reductant and oxidant are constantly changing, the potential, as given by equation 1.1 also changes over time. In short, if we choose to control the potential, then we must accept the

resulting current, and we must accept the resulting potential if we choose to control the current [1][2].

Therefore, there are only three basic experimental designs: (1) we can measure the potential when the current is zero (Open circuit potential), (2) we can measure the potential while controlling the current (Chronopotentiometry), and (3) we can measure the current while controlling the potential (Cyclic voltammetry).

(1) The open circuit potential, measures the stable potential between the working and reference electrode when the counter electrode is disconnected. Consequently, there is no net current flowing, although depending on the material a small or large exchange current may take place on the surface of the electrode. Open circuit potential is often used to determine the state of charge in a battery, or to determine if there is a change in the surface chemistry or if the system is in equilibrium. It often precedes other techniques as validation that the conditions of equilibrium are met, and to determine the DC bias needed to stay in equilibrium.

(2) Chronopotentiometry is similar to open circuit potential, it measures the potential of the WE with respect to the RE while a fixed current is being forced through the WE to the CE. If this current is set to zero it is within the

precision of the control loop – the same as OCP. The technique is often used to characterise batteries at a fixed rate of charge or discharge. Chronoamperometry is similar, but here current is being measured at a fixed potential. Many (gas) sensors operate in this mode, where the presence of certain species gives rise to a current proportional to the concentration.

(3) Cyclic voltammetry is a technique widely used to identify the presence of specific active species, as each redox-couple has a characteristic set of potentials for oxidation and reduction. By sweeping the potential linearly in one direction, then immediately after swept it back (a full cycle) it is possible to deduce the presence of active species, which potential they are active at, and whether there are other relevant reactions (e.g. purely chemical reactions which consume reaction product) [2][3].

In this study, we take CV measurement as an electrochemical reaction analyzing method and section 3.2 has detailed description.

1.2 In-situ TEM observation of electrochemical reaction

In electrochemistry, understanding the mechanism of reaction at the interface of electrode-electrolyte is very important especially in nano-scale. During electroplating or coating, small islands form and afterward those turn into a thin layer. As the energy storage devices like lithium-ion battery or fuel cell, dendrite structures or SEI (solid electrolyte interface layer) formation would determine the performance of devices.

Several groups conducted both visualizing and measuring the reaction of the interface of electrode-electrolyte through in-situ TEM observation [4][5]. In-situ investigation of specimens in liquid that scanning transmission electron microscopy observation of whole cells in liquid [6] and electroplating happened between gold electrodes in liquid cell [7]. In-situ transmission electron microscopy observation of crystallization and nucleation of nanoparticles in liquid to clarify the growth mechanism [8][9][10]. transmission Electroplating and stripping of metal in liquid cell were investigated via in-situ transmission electron microscopy [11][12]. Historically, Ross et al. of IBM firstly achieved such observations [5], White et al. has visualized and analyzed the lead dendrites in aqueous solution in-situ TEM [13]. Oshima et al. developed a new

type of electrochemical cell for TEM observation, which was more conventional than the previous one and observed thin copper (Cu) coating process (Figure 2) [14]. Sacci et al. utilized electrochemical cell for in-situ TEM to analyze lithium dendrite nucleation and SEI formation at the edge of a gold working electrode during electrodeposition (Figure 3) [15].

Figure 2 shows the work of Oshima et al. [14]. The electrochemical cell was consisted of 3 electrodes, working electrode and reference electrode were made of Au film and counter electrode was made of Cu wire, chose dilute H_2SO_4 aqueous as liquid electrolyte.

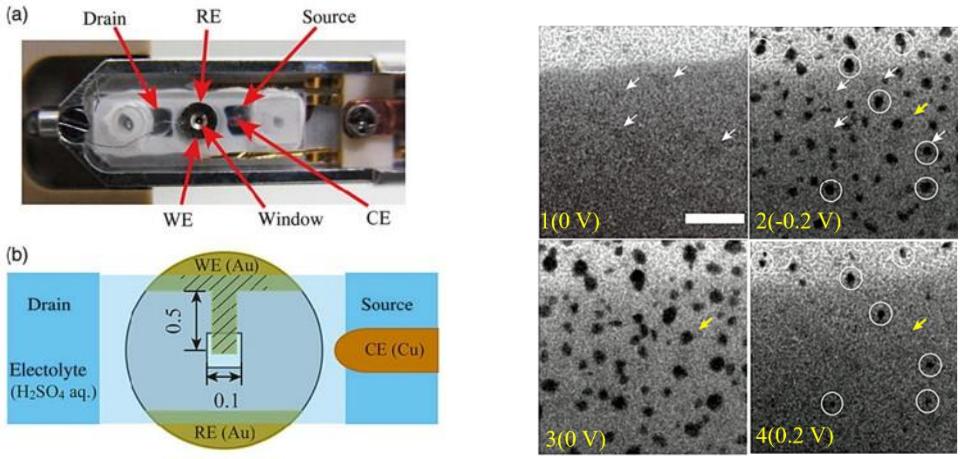

Fig. 2. (a) A photograph of the electrochemical cell (b) Schematic illustration of the electrochemical cell. 1-4 is the growth and stripping processes of Cu islands on Au electrode. Cu islands grew at the negative bias voltage, while they were dissolved at the positive one. [14]

Figure 3 shows the work of Sacci et al. [15]. Fig.2-A is the spacer microchip with a patterned layer of SU-8 used to control fluid thickness and to define a liquid electrolyte flow path. B is the electrochemical microchip with micro fabricated Au electrodes. C is the stacked microchips to create the electrochemical cell and seal battery electrolytes. D is the cross-sectional illustration showing the containment of the electrolyte between the two microchips.

E-H are several individual frames extracted from the in-situ TEM observation video of lithium dendrite nucleation and growth from the Au WE during electrodeposition in the 1.2 M $LiPF_6$ EC/DMC electrolyte. D1-D4 shows that growing speed of lithium dendrite and approximately same.

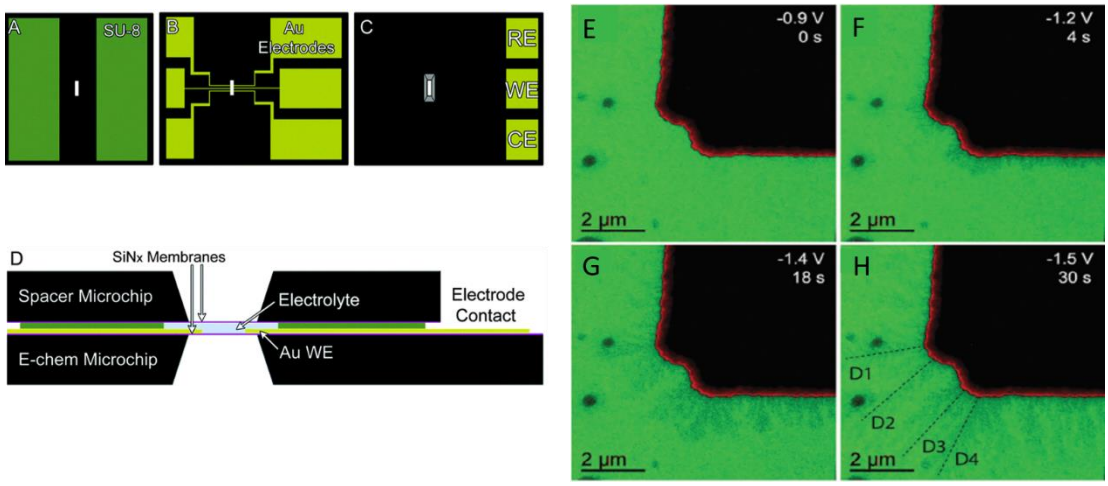

Fig. 3. (A-D) Schematic illustration of the in-situ electrochemical cell components. (E–H) BF-TEM images of lithium dendrite nucleation at the edge of WE during electrodeposition. [15]

However, their work focused on the formation and morphology of dendrite or coating and pursued inadequately about crystallization site differences. Crystallization during electrochemical reaction occurred upon the electric double layer that was determined by not only applied voltage and ion

concentration in aqueous electrolyte but also local structure and morphology of electrode. Electrochemical cell of in-situ scanning electron microscopy observation for electrochemical reaction was developed to conduct visualization of electrode-electrolyte interfaces in real time [16]. In-situ scanning electron microscopy observation of the interfaces of the electrode-electrolyte were achieved [17][18] and the morphological and growth mode during nucleation and crystallization of electrochemical deposition were successfully observed [19][20][21].

Seeing phenomena in liquid at high resolution is crucial in broad areas of biology and materials science and technology [22]. Recently, electron microscope observation with high-resolution in liquid has attracted much interest for biological materials, synthesis of nanoparticles, electrochemical reactions, and so forth [9][23-24][26-33]. For example, de Jonge et al. successfully imaged labeled single molecules on a fibroblast cell with a resolution of several nanometers using a liquid scanning transmission electron microscope (STEM) [34]. Zheng et al. investigated nanoparticle growth in liquid with nanometer resolution using a transmission electron microscope (TEM) [8]. Williamson et al. studied the dynamic processes at solid–liquid interfaces by combination of electrical biasing with a liquid TEM [5]. As for

liquid EM observation, in-situ liquid TEM observation helps us to deeply understand dynamic chemical reactions on a nanoscale [35][36]. For example, White et al. visualized and analyzed lead dendrite formation in aqueous solutions with an in-situ TEM [2]. Sacci et al. utilized an electrochemical cell for an in-situ TEM to analyze lithium dendrite nucleation and solid electrolyte interface (SEI) formation at the edge of a gold (Au) working electrode during electro-deposition (electrodeposition) [15]. These works focused on the formation and morphology of dendrites and pursued the site difference of crystallization and deposition. Meanwhile, it is noted that the electron beam of TEM could induce deposition of dissolved substances, which was not neglected in the dynamic processes of electrochemistry [37]. Furthermore, it is not straightforward to prepare thin liquid films for electron beams to penetrate, which is indispensable for high-resolution TEM observation. On the other hand, in-situ scanning electron microscopes (SEM) were used to observe depositions (depositions) formed on the surface of a thin electron window, which was the opposite side to the electron beam incidence; the secondary electrons emitted from the deposits passed through the window to reach the secondary electron detector of the SEM. For example, Suga et al. reported that deposition of Au and silver on Au electrodes were observed with an inverted atmospheric SEM

[38]. The group of Mølhave reported that, using a standard SEM, electroless deposition of nickel and electro-deposition (electrodeposition) of cupper (copper) on platinum electrodes were observed through a specially microfabricated electron window of a thin (50 nm) Si-rich silicon nitride (SiNx) film [16][39]. Orsini et al. studied the interfaces of plastic lithium battery/cell via in-situ SEM and concluded that the morphology of the electro-deposition (electrodeposition) was correlated to current density [17][18]. For SEM imaging of liquid phenomena, there is no requirement for liquid thickness, differently from those in liquid TEM. The view of SEM is wider than that of TEM. Furthermore, effects induced by electron beam irradiation at lower beam energies in SEM would be less compared to those at higher beam energies in TEM.

In the present work, we develop a two-terminal electrochemical cell for a side-entry holder of a high-resolution in-lens field emission SEM. While measuring cyclic voltammograms (CV) using this equipment, we observe electrochemical deposition and stripping of lead (Pb) on an Au electrode (working electrode), the electric potential of which is controlled with a potentiostat with respect to the potential of the other Au electrode (counter

electrode). The morphological change of Pb deposition in the SEM images is discussed in terms of the potential in the CV.

1.3 The problem of in-situ TEM observation

Sample preparation is time consuming with TEM observation; the thickness of sample for TEM is 100 nm. Dimension of the electrochemical cell must be reduced so small that it differs too much from a real battery. The electron beam is so intensive that it could be easily broken the membrane of the TEM grid [40-48]. Talking about difficulties in in-situ TEM observation, I thought in-situ SEM observation is more suitable and developed electrochemical cell for in-situ SEM observation. When the magnification of the TEM image is high, the current density of incident electron beam should be high. Such high electron density sometimes decomposes the electrolyte solution and generates H_2 bubbles. Therefore, low magnification is required. Since TEM image shows 2-dimensional information, it is difficult to understand the process 3 dimensionally [8] [49].

Chapter 2 Purpose of this research

In this study, we developed an electrochemical cell for in-situ SEM to visualize the lead deposition and stripping on the gold electrode directly and compared the observation with CV result.

Operando SEM observation seems to be better than TEM, since the current density is relatively low, and the sample preparation of SEM is easier than of TEM's [50-52]. As concerned with industrial application, nanomaterials such as nanoparticles or nanowires in size with around 100 nm had been mainly synthesized by electrochemical methods.

The spatial resolution of SEM is high enough to investigate the electrochemical reaction for nanomaterials of such a size. Some companies have commercialized the equipment for operando SEM, but they have some disadvantage for laboratory research such as high financial cost, experimental limitation and so on. Clarifying the correlation of cyclic voltammogram between laboratory and industrial level quantitatively would improve the research work about energy storage device or industrial application of electrochemical reaction such as thin coating or synthesis of functional

materials. Challenge to visualize the electric double layer at the interface of electrode and liquid electrolyte would be meaningful in science.

Chapter 3 Experimental method

We used a high-resolution in-lens cold field-emission SEM (S-5200, Hitachi High-Tech Corporation) having a side-entry holder tubulated in an outer diameter of 8 mm, similar to the holder of TEM. The vacuum of the SEM chamber was able to reach 10−6 Pa; this is benefitable to avoid carbon contamination deposition induced by the electron beam of SEM. The achievable resolution of this SEM was 0.5 nm for Au particles at an acceleration voltage of 30 kV. We developed a compact electrochemical cell with two electrode terminals, as shown in Figure 4, so as to fit into the SEM holder. The holder was specially equipped with multiple vacuum-sealed current feedthroughs for electric measurements. The potential between the working and counter electrodes in the cell was controlled with a potentiostat (VersaSTAT4, Princeton Applied Research); the outputs for the counter and reference electrodes of the potentiostat had connected each other for simple two-terminal electrochemical measurements.

Figure 4 (a) shows the cross-sectional schematic of the developed electrochemical cell. As shown in Fig. 4 (b), the cell was composed of a couple of a cell body (Fig. 4 (c)) and a cell cover (Fig. 4 (d)) of stainless steel, a PEEK

insulator, inner and outer O-rings, and a commercial SiN membrane TEM window grid (4096SN-BA, 3 mm in diameter, 200 μm thick, with a 50-nm thick SiN window of 100 μm × 100 μm in length and width, ALLICANCE Biosystems, Inc., Fig. 4 (e)). These were assembled using four small screws, and the assembled cell was fixed to the end of the SEM holder using a screw and two plate springs. The inner O-ring was pressed between the cell cover and the grid supported by the PEEK insulator onto the cell body. The outer O-ring between the cell cover and the cell body was to seal the electrolyte. The top surface of the PEEK insulator had a dip as a vessel for electrolyte and two trenches, along which two Au wires with a diameter of 0.25 mm were set. The two Au wires encapsulated by Kapton tubes were inserted through two holes on the right side of the PEEK insulator, in Fig. 4 (c), and also through the respective two holes of the cell body. The respective holes of the PEEK insulator and the cell body were aligned on a line. The naked ends of the two Au wires reached the center of the dip. The respective ends of Au wires in the cell were contacted to the working and counter electrodes of Au deposited films formed on the backside of the grid, by being pressed together with the grid and the others using the four small screws. The other sides of two Au wires were connected to the current feedthroughs of the SEM holder using Teflon coated coaxial fine cables.

The two Au wires with the Kapton tubes were bonded to two holes of the cell body using epoxy resin (Torr Seal, Varian), respectively, to prevent the leakage of electrolyte. The cell body had a tiny hole on the front side to release the extra volume of electrolyte when the cell was assembled after injection of the electrolyte onto the dip of the PEEK insulator. The hole was sealed with the epoxy resin immediately after the cell was assembled. A saturated aqueous solution of 1.0 M Pb(NO3)2 was used as an electrolyte in this study.

At the thin SiN membrane window, the film of Au working electrode, formed on the backside of the grid, had a narrow rectangular region at the end of the film, which was as wide as the window and covered the half of the window (Fig. 4 (e)). We deposited Au films for electrodes using DC magnetron sputtering by placing a patterned metal plate as a mask on the grid. Two types of masks with were used, resulted in different sharpness at the edge of the Au deposited film. The end of Au working electrode was observed by the SEM through the membrane window of the grid (Fig. 4 (a)), where the electrochemical reactions took place. For observation of electrochemical deposition and stripping, the SEM was operated at an acceleration voltage of 10 kV at an emission current of 10 μA. The incident current into the cell was 10 pA, which was separately measured using a custom-made Faraday cup. Each SEM image was taken at a

slow scan mode of 8.4 sec/frame. While the consecutive SEM images were being captured with a video capture board in a computer, the CV was measured with the potentiostat in a sweeping range from +2 to −2 V at a scan speed of 50–60 mV/s. The output of the potentiostat was applied to the working electrode while the counter electrode was electrically grounded, and the electrochemical current was recorded through the software to control the potentiostat.

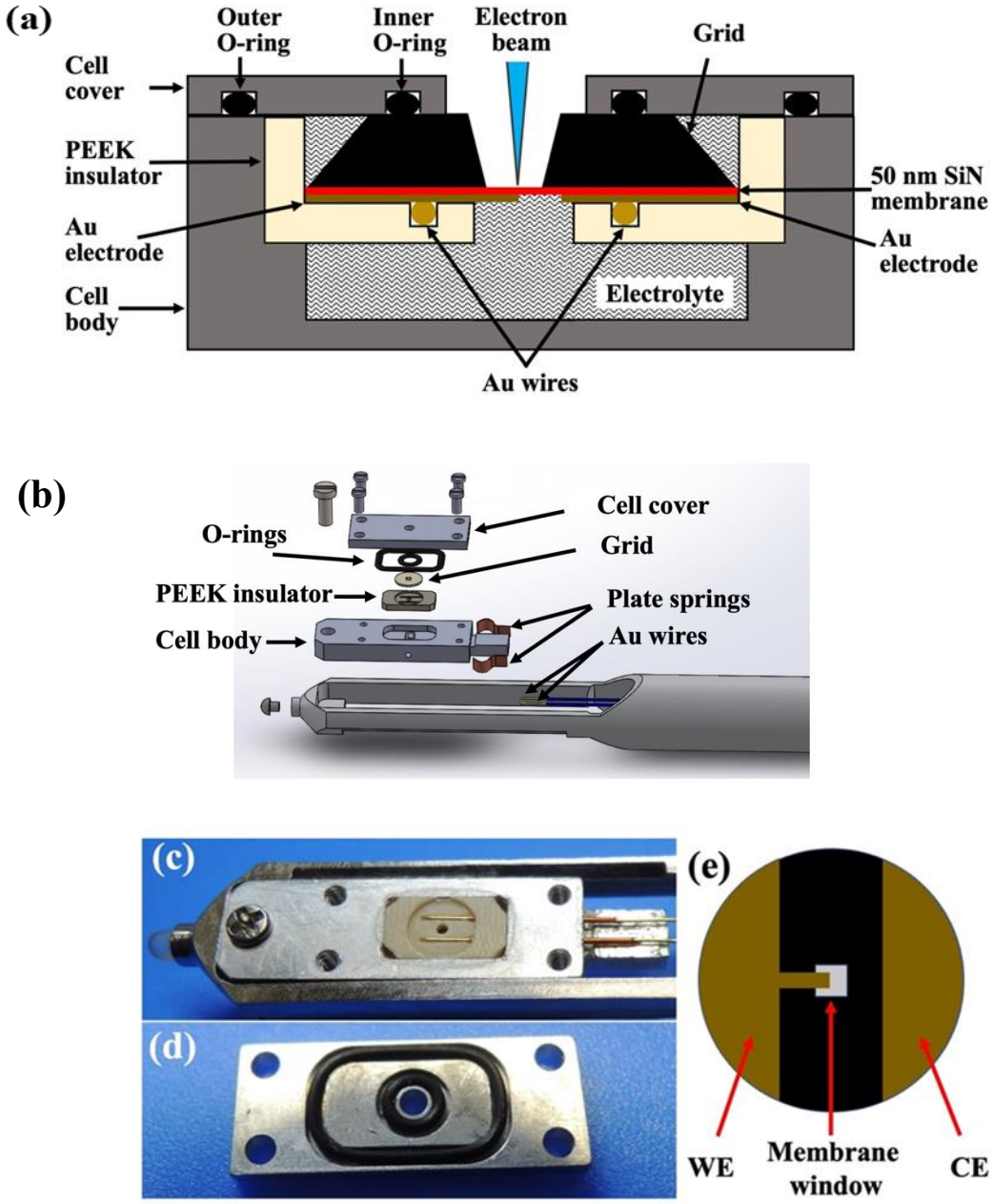

Fig. 4. (a) Cross-sectional schematic of the electrochemical cell. (b) Exploded view of the electrochemical cell, composed of the cell body, the PEEK insulator, the grid, two O-rings, and the cell cover. (c) Photo of the cell body, the PEEK insulator, and the two Au wire, which were assembled and fixed onto the end of the SEM holder. (d) Cell cover, inner and outer O-rings. (e) Schematic of the

grid with a SiN membrane window and the Au deposited films for the working electrode (WE) and the counter electrode (CE).

3.1 Scanning Electron Microscope (SEM)

The limit of resolution of naked eye is around 0.1 mm and can distinguish object like human hair, also can see the structure of small object about 1 μm like bacteria by optical microscope. Electron microscope has higher resolution power than light microscope and can obtain rigorously information about nanoscale. It utilized the accelerated electron beam that has much shorter wavelength than visible light as illumination source. There are two kinds of electron microscope, such as transmission electron microscope (TEM) and scanning electron microscope (SEM).

TEM uses an accelerated electron beam to transmit the sample and achieve an image. The electron beam is generated by an electron gun. The energy between anode and cathode that accelerate the electron beam is typically +100 keV. TEM focusses the electron beam with electrostatic and electromagnetic lenses and transmit through the sample. Part of the sample is transparent to electrons and the other parts scatters them out of the beam. Objective lens system of the microscope magnifies the structural information of the sample which is carried by the electron beam after it transmit through the sample.

The SEM produces images by raster scanning the sample with a focused electron beam. There are several kinds of energy lose mechanism when the electron beam illuminates the sample. The lost energy is converted into alternative forms such as heat, emission of low-energy secondary electrons and high-energy backscattered electrons, light emission (cathodoluminescence) or X-ray emission [44], all of which provide signals carrying information about the properties of the specimen surface, such as its topography and composition. The SEM image is the varying intensity of any of these signals from a position corresponding to the position of the beam on the specimen where the signal was generated. Generally, the image resolution of SEM is lower than that of TEM. However, because the SEM scan the surface of a specimen rather than its interior, the electrons do not have to transparent through the specimen. This reduces the need for extensive sample preparation to thin the specimen to electron transparency. The SEM can image bulk samples that can fit on its stage, including a height less than the working distance being used, often 4 millimeters for high-resolution images. The SEM also has a great depth of field, and so can produce images that are good representations of the three-dimensional surface shape of the sample. There are two main lenses used in SEM, as condenser lenses and objective lenses. Condenser affects the number of electrons in the

beam for a given objective aperture size, and the objective lens focuses electrons on the sample at the working distance. Lens strength could vary when adjusting the amount of current, which flows through the windings around the iron core of the magnet.

As the main equipment throughout this work, Hitachi S-5200 FE-SEM (Figure 5) is capable of high- resolution observation by inserting the specimen into the objective lens; also emphasize the composition information and surface information of high-resolution region through controlling the SE and BSE.

Here present the main specification and the schematic diagram of Hitachi S-5200 FE-SEM (Figure 6).

SE resolution	0.5nm (30kV)/ 1.8nm (1kV)
Magnification	60～2,000,000
The maximum sample size	5.0mm×9.5mm×3.5mm (plane sample) 2.0mm×8.0mm×5.0mm (sectional sample)

Fig. 5. Hitachi S-5200 Field Emission Scanning Electron Microscopy

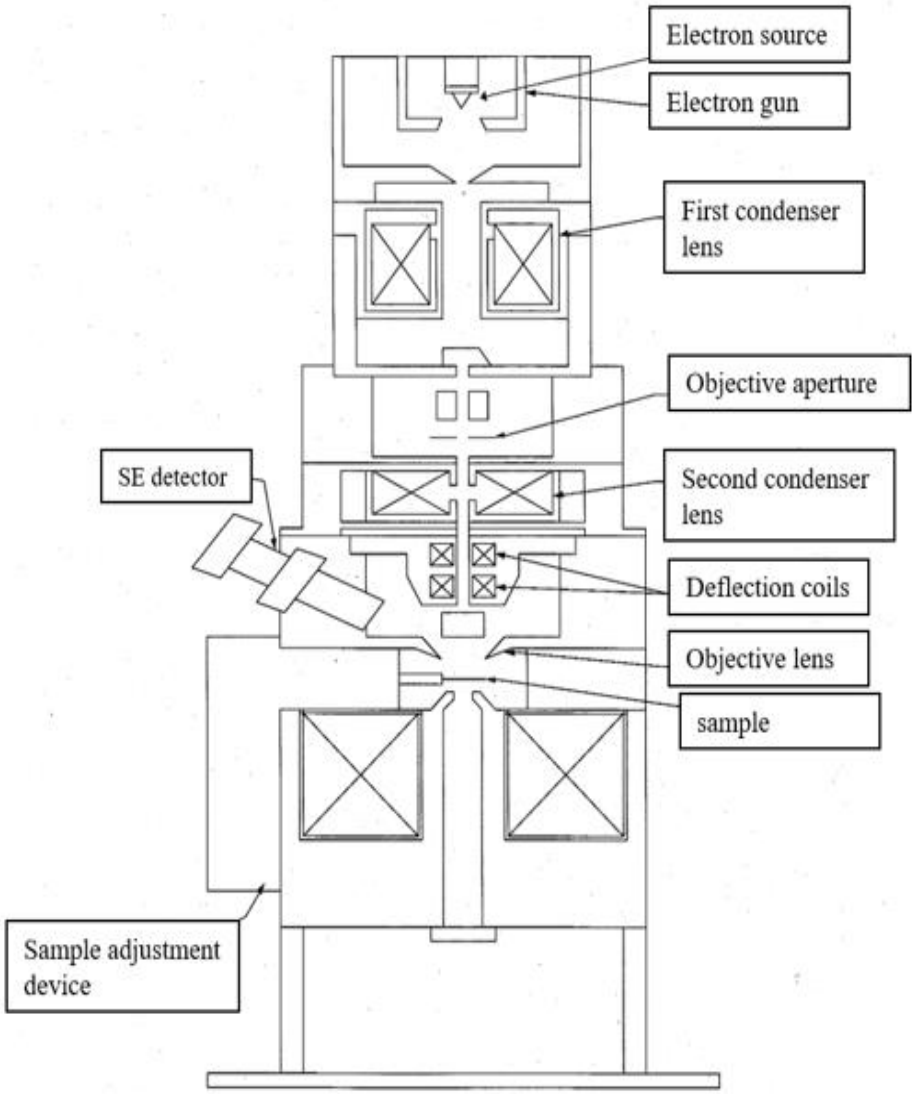

Fig. 6. Schematic diagram of Hitachi S-5200 FE-SEM [this is taken from manual of Hitachi S-5200 FE-SEM].

When incident electrons (primary electron) penetrate the surface of the solid sample, provoke elastic collision, scattering (elastic scatter) and inelastic scattering because of the influence of the potential energy of the atoms constituting the solid sample. When primary electrons are inelastically scattered by collisions with atoms in the solid, if the energy of the excited electrons is larger, and this scattering process occurs near the surface, also part of the energy is lost and depart the surface as drifting, these electrons called secondary electron (SE). On the other hand, in the case of elastic scattering, if emission electron has very large scattering angle or take the path in the opposite direction to the incidence after several scattering and emitted from the sample surface almost same position with irradiation position of the incident electron, these electrons called backscattered electrons (BSE). Transfer of energy during inelastic scattering is distributed to not only energy loss of primary electrons and generation of secondary electrons but also emission of cathode luminescence light and X-rays when electrons move from excited state to low energy state. Figure 7 shows a schematic diagram of the interaction between electron beam and solid sample surface.

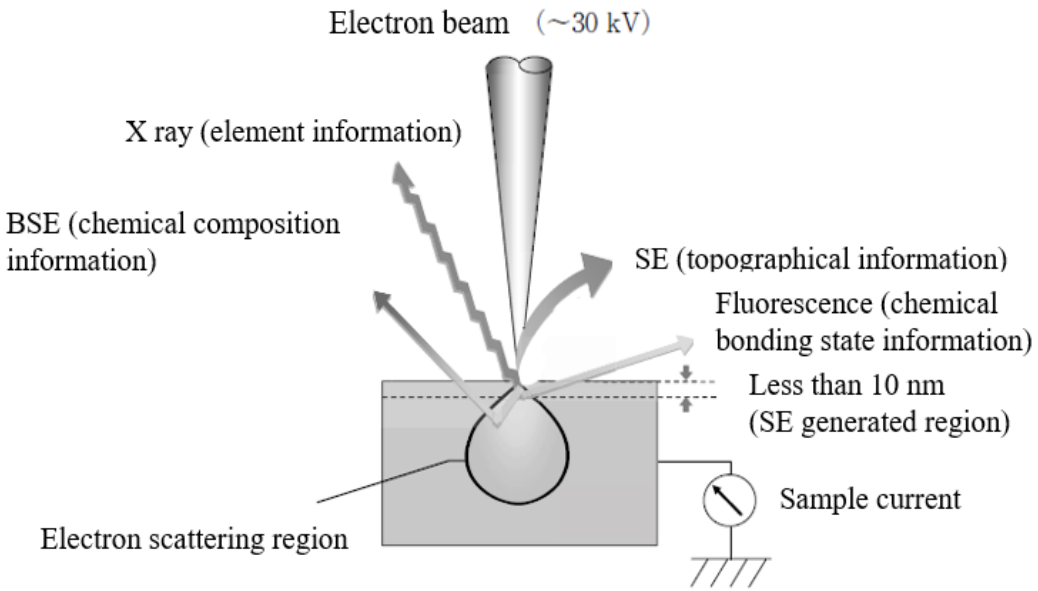

Fig. 7. Schematic illustration of electron beam and specimen surface interaction mechanism. [53]

3.2 Cyclic voltammetry

There are three main electrochemical measurement methods as well as potentiometric method, coulometric method, voltametric method.

With the potentiometric method, potential of one electrode is fixed and analyse the electrochemical reaction through correlation between potential of electrochemical cell and concentration of reactant in the cell.

$$E_{cell} = E_c - E_a$$

From Nernst equation

$$E = E^0 + \frac{RT}{nF}\log Q$$

E^0*: standard electrode potential*

R: gas constant

T: temperature in kelvins

n: number of electrons in the reaction

F: faraday's constant

Q: reaction quotient

With the coulometric method, complete electrolysis of analyte-comletely oxidized or reduced at working electrode or react with reagent generated at working electrode. There are two types of methods as controlled-potential coulometry that appy constant potential to electrochemical equipment and

controlled-current coulometry that pass constant current through electrochemical equipment. The coulometry is used for quantitative analysis of both organic and inorganic analyte. The controlled-potential coulometry analyses involves the determination of inorganic cations and anions, including trace metals and halids ions. The controlled-current coulometry (coulometric titrations) has two advantages compared to conventional titration. It is hard to prepare and store a solution of highly reactive reagent, such as Ag^{+} and Mn^{+}, but generate them electrochemically and use them in a coulometric titration. Also, it is relatively easy to measure a small quantity of charge, to analyze an analyte whose concentration is too small for conventional titration. Direct oxidation of reduction of protein at a working electrode is difficult if the active redox site of the protein lies deep within its structure.

With the voltammetry method, measure the current that flowing between the working electrode and the counter electrode of electrochemical cell when the time-dependent potential between the working electrode and the reference electrode of same cell is varied. The data obtained from the resulting current produced by the analyte versus applied potential of the working electrode called voltammogram. There are several kinds of voltammetry method depend on the potential control mode, such as linear sweep voltammetry, staircase

voltammetry, squarewave voltammetry, cyclic voltammetry, stripping voltammetry, alternating current voltammetry, polarography, rotated electrode voltammetry, pulse voltammetry and so on.

In linear sweep voltammetry, information about electrochemical reaction is introduced by measurement of the current at working electrode when the applied potential of the electrochemical cell is swept linearly. The peak or change in the current plot appeared at the redox potential would give the information of desired reagent. Like this method, the staircase voltammetry, the potential is swept in a form of stair steps, and the current is measured at the end of every step. The square wave voltammetry is one of the linear sweep voltammetry, potential is swept in the form of combination of square wave and staircase potential. The stripping voltammetry is the analytical method that used to quantitative analysis of trace element in organic or inorganic compound. The alternating current voltammetry is an analytical method used for electrochemical cell that using oscillating voltage to the electrochemical reaction. In the polarography method, using dropping mercury electrode as the working electrode and current was related to the mass of mercury drop. In the rotated electrode voltammetry, the working electrode is made of noble metal or glassy carbon and will rotate in certain angular velocity during redox reaction.

The pulse voltammetry method can be considered as the combination of linear sweep voltammetry and staircase or square wave voltammetry and used in analysis of extremely small amounts of analyte.

CV measurement is a commonly used electrochemical measurement technique to study the electron transfer-initiated chemical reactions. Through impose a set of bias voltage to electrochemical system and measure the electric current passed. Generally, x-axis represents the applied potential (E) and y-axis represents the measured electric current (I). By sweeping the potential linearly in one direction, then immediately after swept it back (a full cycle) it is possible to achieve the current variation numerically. Parameters like sweeping speed (scan rate) and direction, magnitude of applied voltage, concentration of reactant would influence the shape of cyclic voltammogram (potential-current plot achieved from CV measurement). Current variation can imply the quantity of electron transfer during reduction and oxidation processes and relate the potential value to the presence and consumption of chemical compound. Take electroplating as example, by observing the growth and strip of dendrite or crystal island and conduct a CV measurement simultaneously, can get what potential value the electroplating occur and what potential value it will disappear [22].

Take Nernstian equilibrium between ferrocenium (Fc+) and ferrocene (Fc) as example to explain the relationship between cyclic voltammogram and electrochemical reaction.

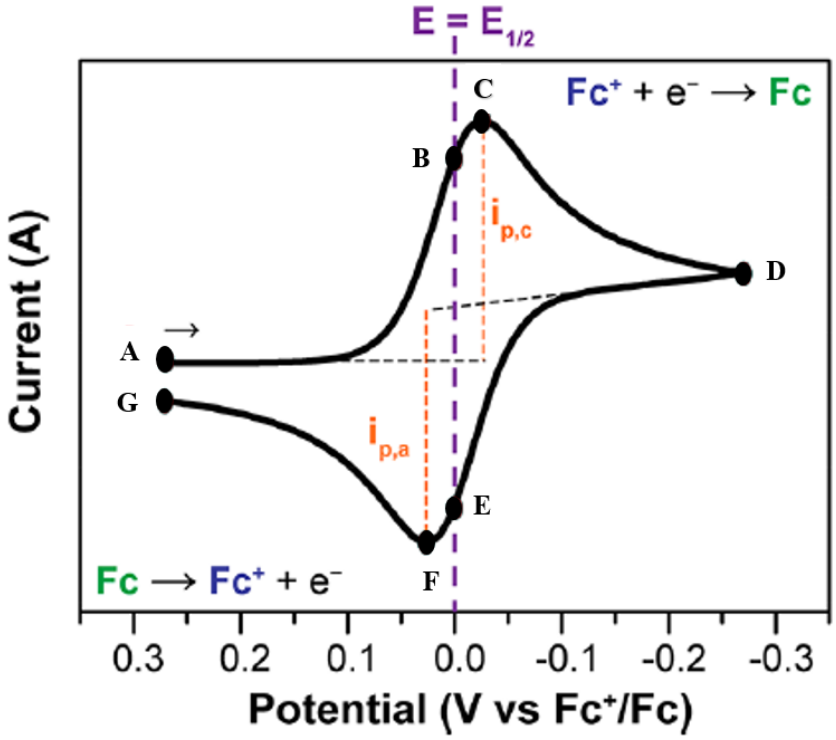

Fig. 8. Typical cyclic voltammogram of electrochemical reaction (the reversible reduction of a 1mM Fc+ solution to Fc, at a scan rate of 100 mV s−1).[1]

As shown in the figure 8, concentration of Fc^+ decrease near the electrode as it is reduced to Fc when scan the potential negatively between point A and point D. The peak cathodic current (i_{pc}) is observed at the point C and it is caused by the delivery of Fc^+ via diffusion from the bulk solution. The diffusion layer is

the volume of solution at the surface of the electrode and containing the reduced Fc. It continues to grow during whole scanning process. This slows down mass transport of Fc^+ to the electrode. When scan the potential negative direction, slow down the diffusion rate of Fc^+ from the bulk solution to the electrode surface and lead to a decrease in the current as the scanning process continues ($C \rightarrow D$). When the potential is reached switching potential (D), the scan direction is reversed, and the potential is scanned in the positive (anodic) direction. While the concentration of Fc^+ at the electrode surface is decreased and the concentration of Fc at the electrode surface increased, satisfying the Nernst equation. The Fc appear at the electrode surface oxidized back to Fc^+ as the applied potential becomes more positive. At points B and E, $[Fc^+]$ and [Fc] at the electrode surface are equal, following the Nernst equation, $E=E_{1/2}$ this corresponds to the halfway potential between the two observed peaks (C and F). The two peaks are separated because of the diffusion of the analyte to and from the electrode [1][45].

The sweep rate of the experiment decides how fast the applied potential is scanned. Faster scan rates lead to a decrease in the size of the diffusion layer; therefore, higher currents will be observed. For electrochemically reversible electron transfer processes involving freely diffusing redox species, the

Randles−Sevcik equation (equation 3.2.1) describes how the peak current i_p (A) increases linearly with the square root of the scan rate υ (V s^{-1}). Where n is the number of electrons transferred in the redox event, A (cm^2) is the electrode surface area (usually treated as the geometric surface area), D_0 (cm^2 s^{-1}) is the diffusion coefficient of the oxidized analyte, and C^0 (mol cm^{-3}) is the bulk concentration of the analyte.

$$i_p = 0.446 \times 2\mathrm{FAC}^0\left(\frac{2F\upsilon D_0}{RT}\right)^{1/2} \qquad 3.2.1$$

3.3 Electrochemical cell

We developed an electrochemical cell for in-situ SEM observation, the cell is sized to fit into the tip of the specimen holder and two Au wire inserted its side through two holes. At the observation area, there is a through-hole to the electrochemical cell, which is filled with electrolyte solution. On the front plane of the cell body, insulator has a concentric hole, and two trenches allows for the insertion of the Au wires up to close of the observation hole. When insert the silicon nitrate TEM grid with two vapor deposited electrode into the cell, electrical connection and hermetic sealing will be accomplished and electrochemical reaction could occur between these two electrodes. There are two trenches for O-ring, one is smaller than the silicon nitrate grid and the other is larger. It should make sure that electrolyte won't leak during experiment. Observation have been conducted through the concentric hole in the cell-cover. When we vary the applied potential, electrochemical reaction occurs at the electrode surface, allowing me to investigate the relationship between electrochemical deposition and stripping with applied potential and measured current in-situ.

As shown in Figure 9, the electrochemical cell consists of the following parts listed below: (Parts that have been manufactured by an external company based on my design are marked by [*])

Four M1 screw

One M1.4 screw

[*] Cell-cover

Two O-rings

Silicon nitride grid

[*] PEEK insulator

[*] Cell body

Bumper

Two pieces of Au wire covered with Kapton tube

Specimen holder

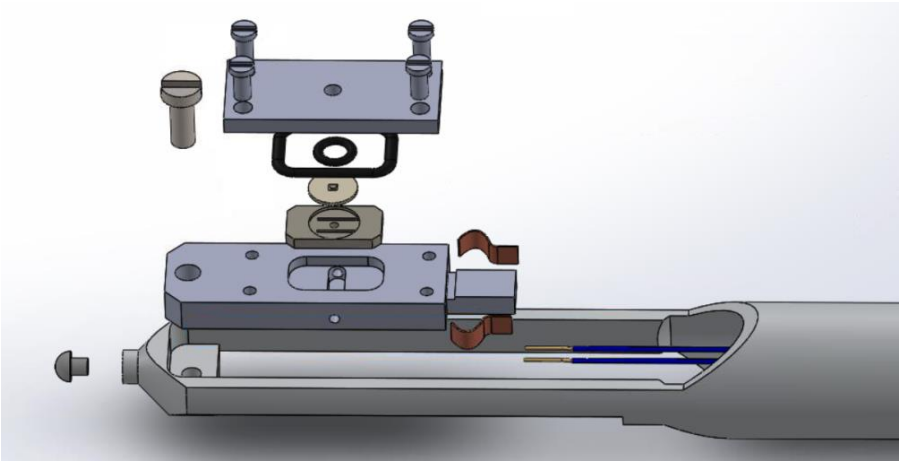

Fig. 9. schematic illustration of exploded view of the electrochemical cell

The cell-cover is rectangle shaped (12.60mm×5.5mm×1mm) and is made of stainless steel as shown in Figure 10. It can be fixed to the cell body with four M1 screws and has a through hole with diameter 1 mm. SEM observation will be conducted through this hole and the cell-cover is symmetric (more stable) around the observation hole. In order to inhibit the leakage of liquid electrolyte between silicon nitrate grid and body, there are two O-ring trenches surrounding the observation hole and symmetric as well to improve the sealing effect.

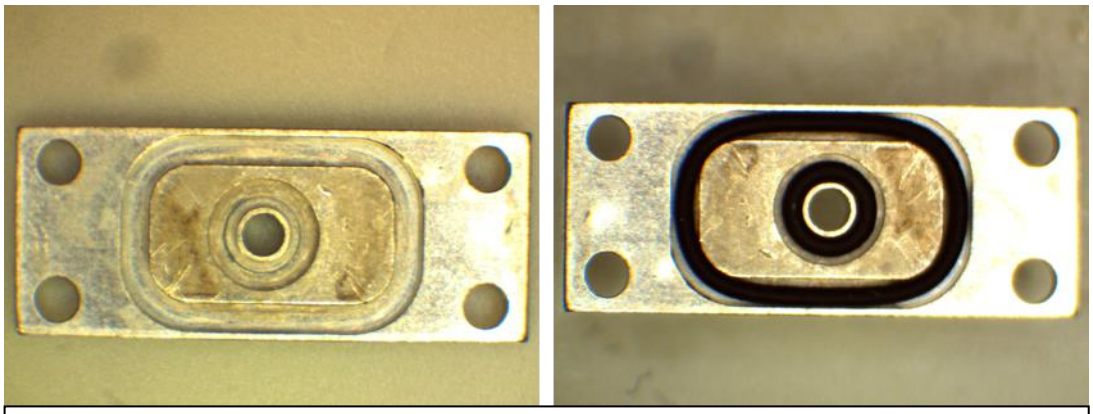

Fig. 10. Electrochemical cell cover

As shown in Figure 11, the insulator is made of PEEK material and placed into the same shaped recess in the cell body. It is symmetric around the observation hole and thickness is 0.7 mm. Place the silicon nitride TEM grid upon circle shaped recess with diameter of 3 mm and depth of 0.2 mm that concentric to the observation hole. Two Au wires which are inserted through the

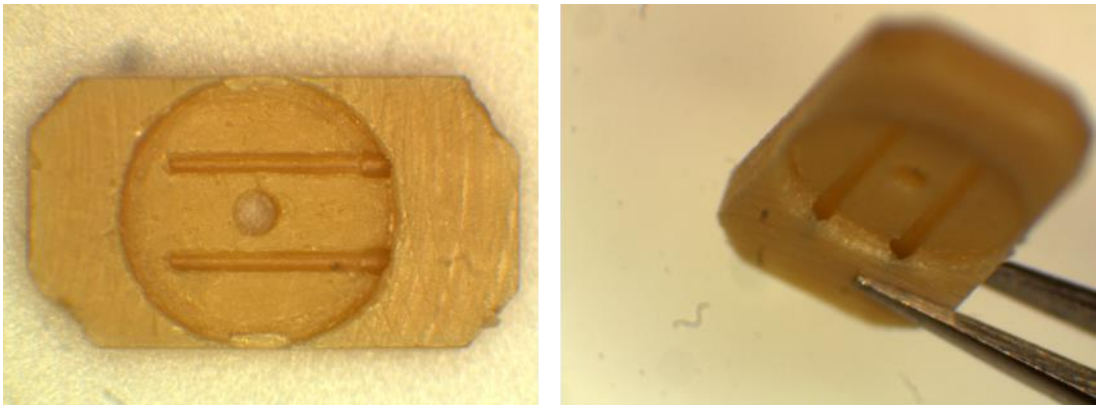

Fig. 11. PEEK insulator

cell body can be inserted into the two closed holes and make contact with two electrode of silicon nitride grid.

Figure 12 shows the body that is made of stainless steel and assembled on the specimen holder tip by one M1.4 screw. There are four M1 screw hole for fixing the cell-cover. Electrolyte will be filled from the hole on the cell side and flew out from the other side, also stage was added allowing the two Au wires to be fixed after inserted into the cell-body.

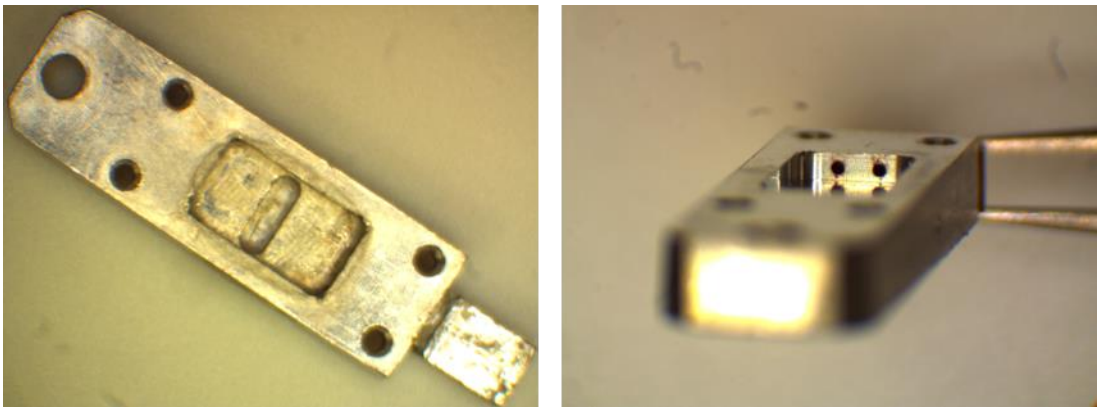

Fig. 12. Electrochemical cell body

There is a 0.7mm deep recess with the same shape as the PEEK insulator. Two Au wire with kapton tube can go through the two holes on the opposite side of fixing part, go through the PEEK insulator and make contact with the TEM grid.

Figure 13 shows the silicon nitride TEM grid with vacuum-deposited Au electrode

Frame thickness	200 μm
Film	20 nm silicon nitride
Window size	100 × 100 μm × 1win
Au electrode thickness	About 20 nm

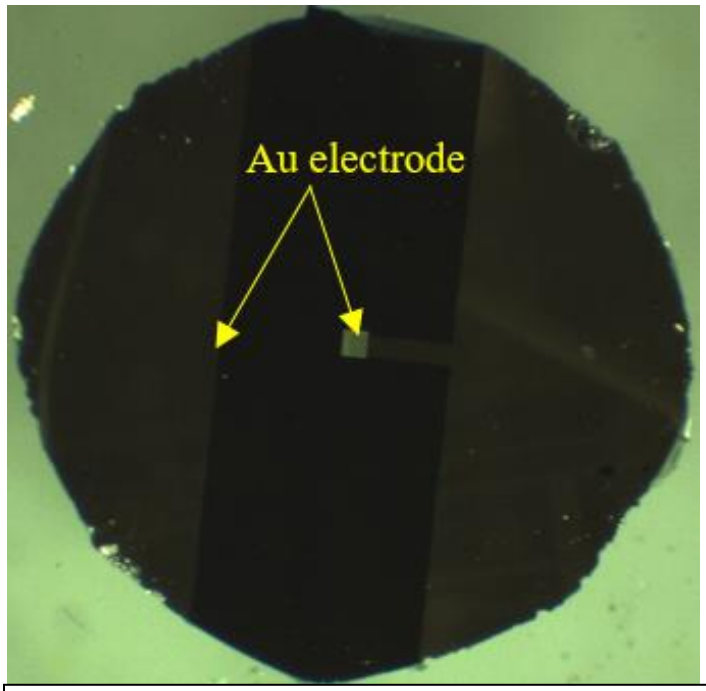

Fig. 13. Silicon nitride TEM grid with Au electrode

The stage (Fig.14 (①)) used for the fabrication of gold electrode onto the silicon nitride TEM grid has a recess part that same size and depth with the grid at the center. The go through small hole in the center would protect the membrane during evacuation that the air pressure difference between outside and inside of grid window part would break the membrane. After placing the grid into the recess part of stage, the mask would be fixed to the stage with four screws. Inserting two needles through the extra small holes before fixing the four screws to prevent the mask move when fastening the screws. The mask 1 (Fig.14 (②))has two rectangular hollow part symmetric to the center of mask, after the sputtering with DC magnetic sputter (Fig.14 (③)), there would be two Au film on the TEM grid (Fig.14 (④)). In order to reduce the gap between mask and grid, we attached 2 mesh to the mask 2 and top view would be like Figure 14 (⑥). Because of the roughness difference of inside surface of drain part of copper mesh and stainless steel mesh, the electrode surface would be smooth after used copper mesh and would be rough after used stainless steel mesh.

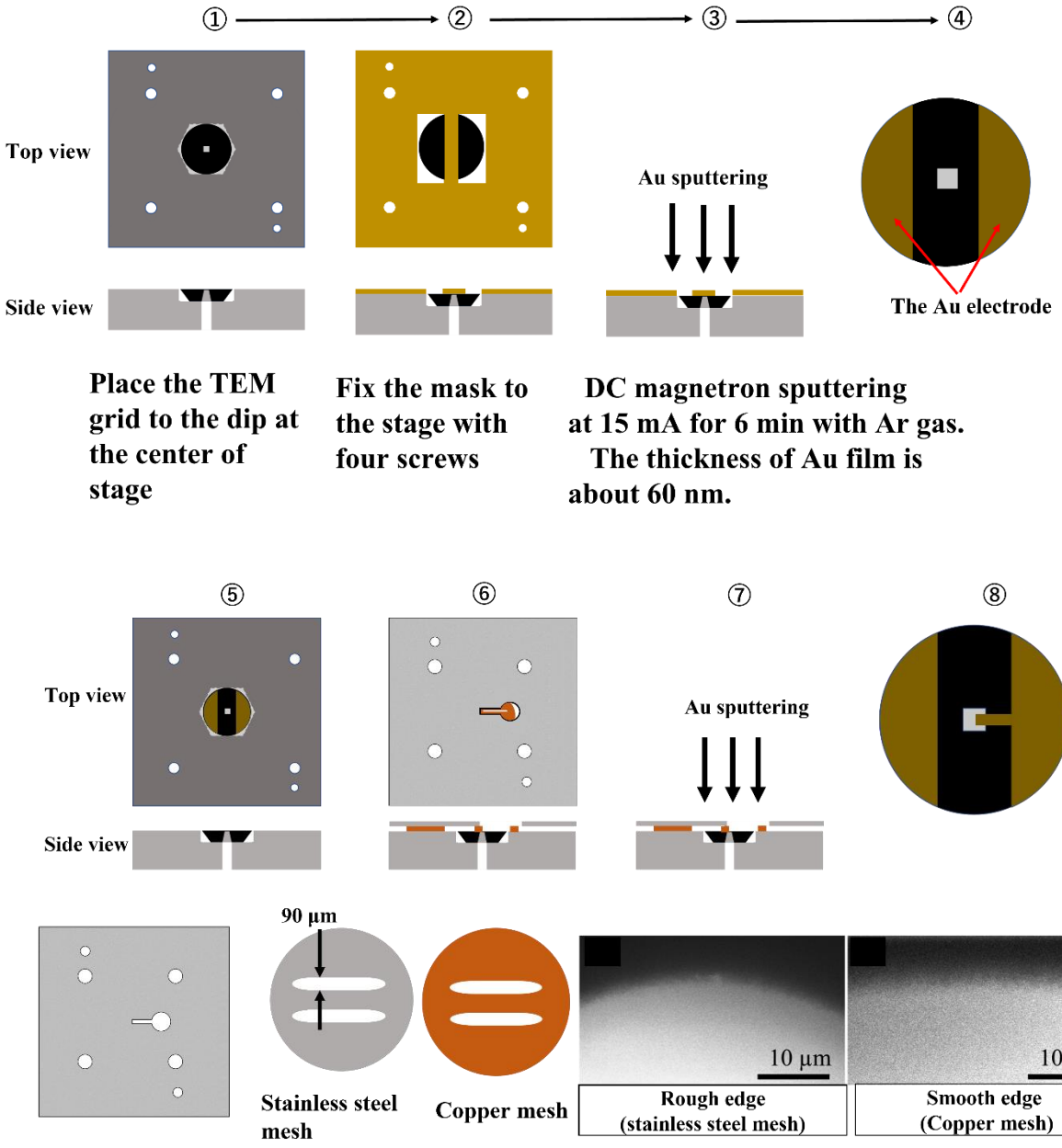

Fig. 14. Fabrication process of Au electrode onto the silicon nitride TEM grid

First assemble the electrochemical cell to the custom-made SEM holder as shown in the figure 15, the two gold wire were connected to the feedthrough parts of the holder and works as the working electrode and counter electrode. These two electrodes were connected to the Galvanotic by cable and CV measurement were controlled by the computer which connected to the Galvanotic , the parameters of the CV measurement were controlled by software VERSus that installed in that computer. Using VERSus, we can set the sweeping voltage range, scan speed, scan cycle number and other parameters. The video of the SEM screen was recorded through software Vrecord which installed in another computer that connected to the SEM directly.

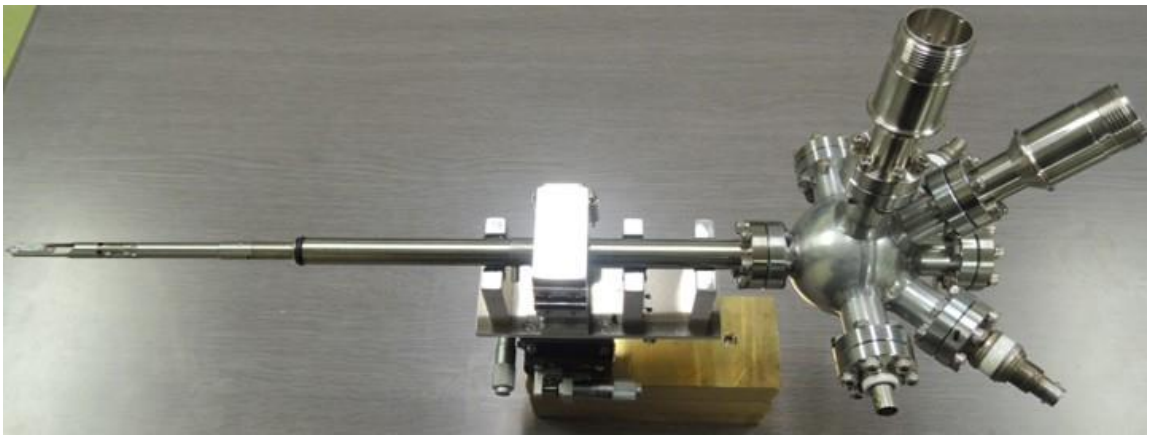

Fig. 15. Specimen holder for Hitachi S-5200Tip of the specimen holder for Hitachi S-5200.

Chapter 4 Results and discussion

4.1 Emission current measurement of SEM using Faraday cup

The Faraday cup is designed to fit into the tip of custom-made SEM holder (Figure 16). It has copper body works as the vessel and circular recess part for metallic part with small hole, under the metallic part, there is semi-circle shaped recess part that works as the faraday cup and its center was deviated from the center hole of metallic part. The cover has a hole at its center which is concentric with the metallic part. Both the cup body and screw that fixing the cover to body were isolated from cover by insulator. So only the electron which reach to the cup bottom would be adsorbed by the cup body and converted into electron current and could be measured. The electron that absorbed by the cup body would be attracted by the 90 V of battery and collected by current amplifier.

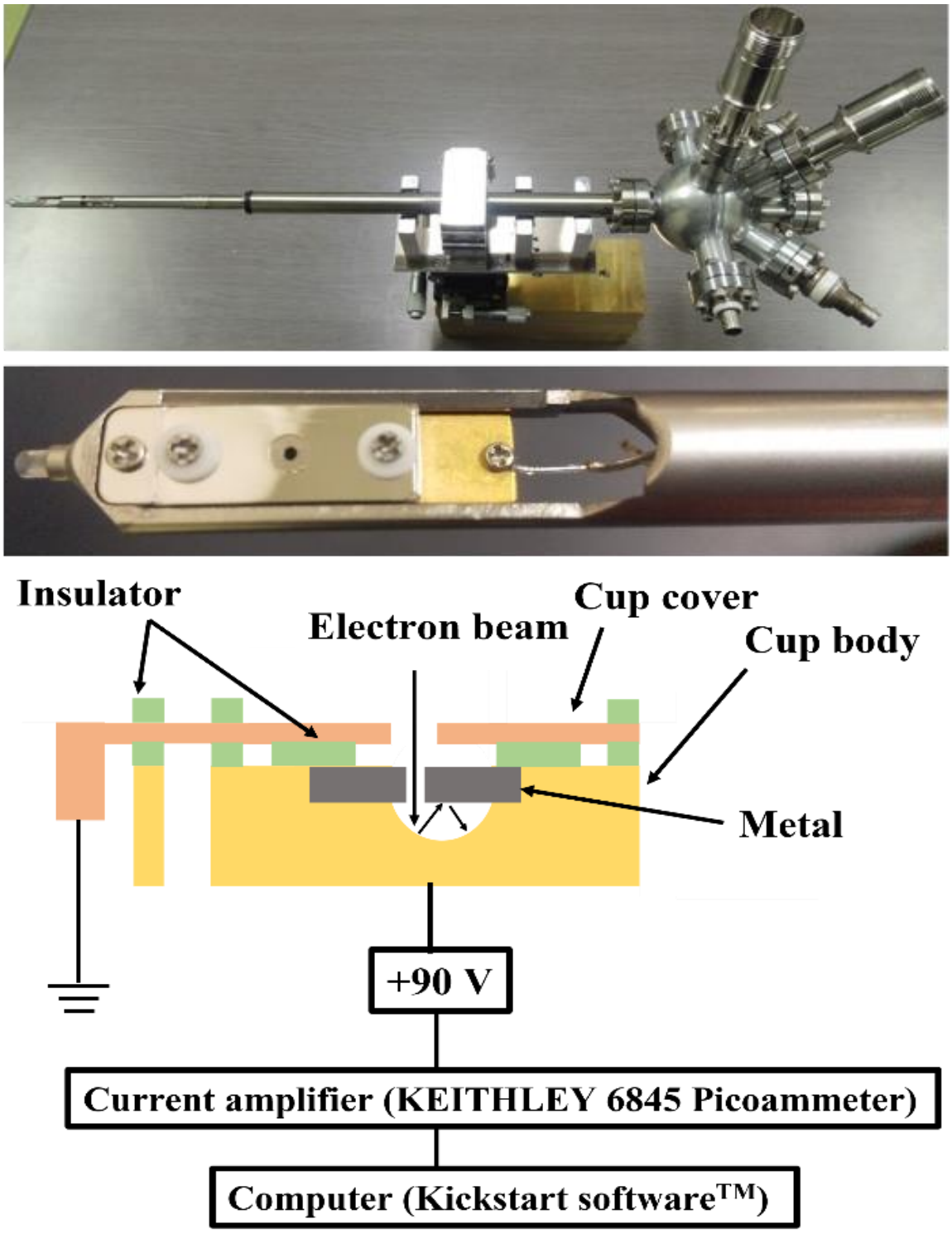

Fig. 16. Schematic diagram and specimen holder for Faraday cup

Fix the acceleration voltage of SEM and vary the emission current as 5 μA, 10 μA, 15 μA, 20 μA, adjust the electron beam to both of inside and outside of faraday cup and measure the current values every each one of the emission current.

For example

5 kV 5 μA inside the hole

5 kV 5 μA outside the hole

5 kV 10 μA inside the hole

5 kV 10 μA outside the hole

Set the number of scanning cycle of the KICKSTART software to 500 and minus I_{out} (for example: the average value from 500 times irradiation outside the hole when 5 kV 5μA) from I_{in} (for example: the average value from 500 times irradiation outside the hole when 5 kV 5μA), consider the obtained value as the actual current value that reached the surface of sample. And the measurement condition of SEM was at Low magnification, scale at 5 μm, resolution at 7.00 K, scan mode: 7 (small window mode). To extract the secondary electron more effectively, applied 95,67 V (battery of 9V×10)

between SEM holder and Picoammeter. First fix the applied voltage of SEM to one of the four values as 5 kV, 10 kV, 15 kV, 20 kV, and then conduct the measurement by adjusting the electron beam with four different emission current as well as 5μA, 10μA, 15μA, 20μA to both inside and outside of the faraday cup hole separately.

For each emission current under different applied voltage, the summarized data was below, meaning of the used symbols would be

- $5\ \mathrm{kV}$: applied voltage
- $\mathrm{I_{SEM}(\mu A)}$: emission current
- $\mathrm{I_{out}(pA)}$: outside the hole
- $\mathrm{I_{in}(pA)}$: inside the hole
- $\mathrm{I-5\ kV(pA)}$: measured current

When applied voltage 5 kV、emission current 5μA

I_out (pA)=−0.42 pA the average value of 500 times irradiation outside the hole when 5 kV 5μA

I_in (pA)=−3.39 pA the average value from 500 times irradiation inside the hole

when 5 kV 5μA

$$I{-}5\ kV(pA)=I\_in\ (pA){-}I\_out\ (pA)$$

5 kV			
$I_{SEM}(\mu A)$	$I_{out}(pA)$	$I_{in}(pA)$	$I-5\ kV(pA)$
5	-0.42	-3.39	-2.97
10	-0.2	-6.18	-5.98
15	-0.29	-8.9	-8.61
20	-0.66	-11.1	-10.44

10 kV			
$I_{SEM}(\mu A)$	$I_{out}(pA)$	$I_{in}(pA)$	$I-10\ kV(pA)$
5	-0.47	-6.45	-5.98
10	-0.54	-10.4	-9.86
15	-0.2	-14.7	-14.5
20	-0.97	-19.8	-18.83

15 kV			
$I_{SEM}(\mu A)$	$I_{out}(pA)$	$I_{in}(pA)$	$I-15\ kV(pA)$
5	-0.49	-8.96	-8.47
10	-0.36	-16.3	-15.94
15	-0.77	-22.6	-21.83
20	-1.15	-29.7	-28.55

20 kV			
$I_{SEM}(\mu A)$	$I_{out}(pA)$	$I_{in}(pA)$	$I-20\ kV(pA)$
5	-0.48	-12.6	-12.12
10	-0.73	-23.1	-22.37
15	-0.97	-33.1	-32.13
20	-1.27	-43.5	-42.23

25 kV			
$I_{SEM}(\mu A)$	$I_{out}(pA)$	$I_{in}(pA)$	$I - 25\ kV(pA)$
5	-1.05	-16.6	-15.55
10	-1.5	-30.1	-28.6
15	-2.1	-42.9	-40.8
20	-2.4	-53	-50.6

30 kV			
$I_{SEM}(\mu A)$	$I_{out}(pA)$	$I_{in}(pA)$	$I - 30\ kV(pA)$
5	-1.06	-22	-20.94
10	-1.51	-40	-38.49
15	-2.13	-56.6	-54.47
20	-2.66	-70	-67.34

Summarize all the measurement data from different emission current (5 μA, 10 μA, 15 μA, 20 μA) under each applied voltage (5 kV, 10 kV, 15 kV, 20 kV, 25 kV, 30 kV)

$I_{SEM}(\mu A)$	I-5kV(pA)	I-10kV(pA)	I-15kV(pA)	I-20kV(pA)
I-5	-2.97	-5.98	-8.47	-12.12
I-10	-5.98	-9.86	-15.94	-22.37
I-15	-8.61	-14.5	-21.83	-32.13
I-20	-10.44	-18.83	-28.55	-42.23

Using the data from table above, we can get the Figure 17 would be obtained, and switching the row and column, will obtain the Figure 18.

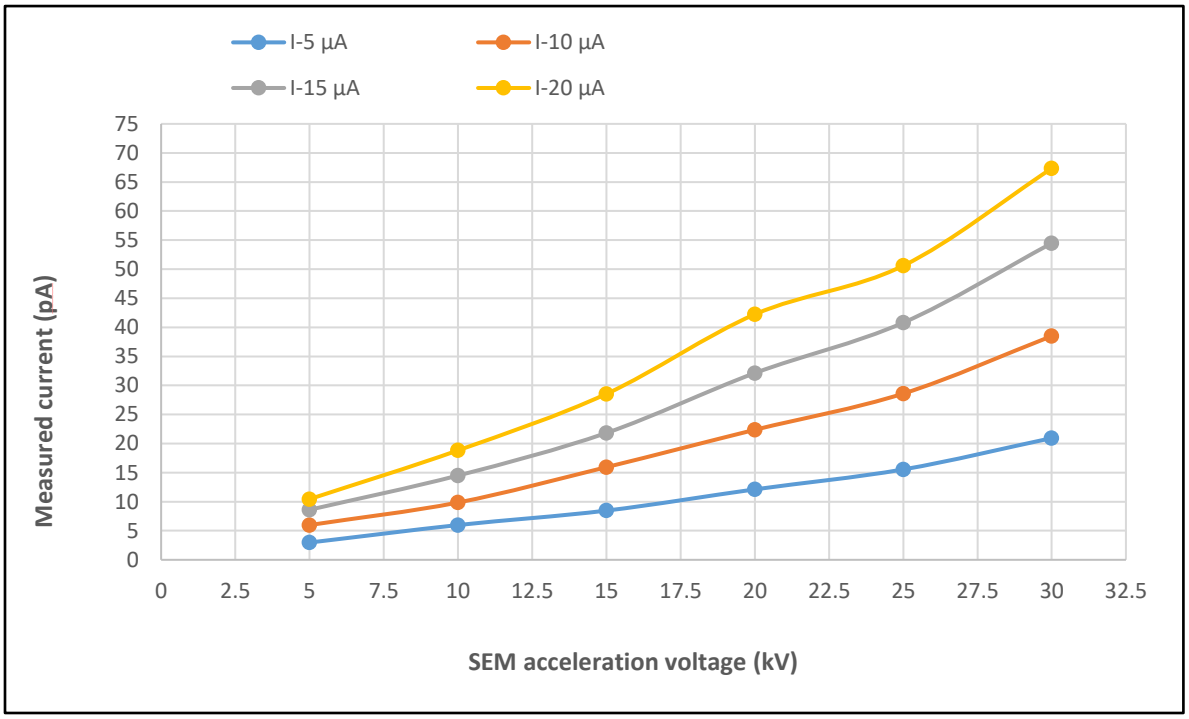

Fig. 17. When emission current is constant, the relation between applied voltage and measurement current

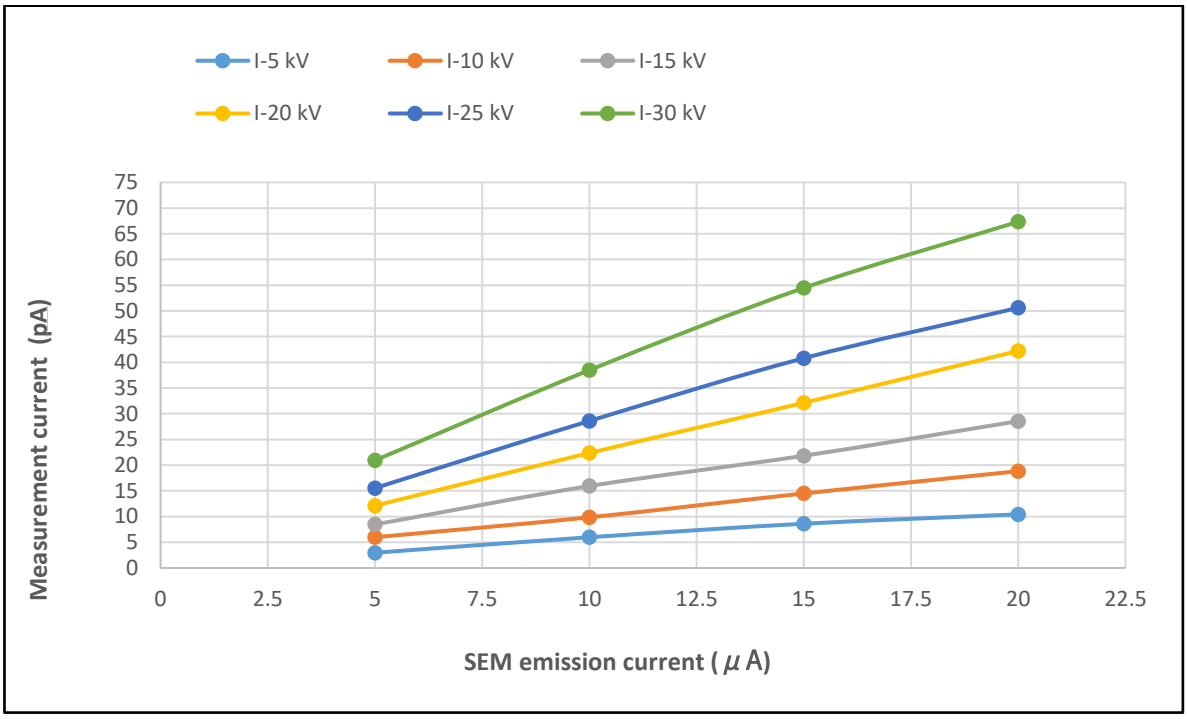

Fig. 18 When the applied voltage is constant, the relation between emission current and measurement current

As a conclusion, the measurement current increase simultaneously with the increase of applied voltage; the measurement current increase simultaneously following the increase of emission current.

4.2 ex-situ observation

Figure 19 shows a series of optical microscope images that were taken from the electrochemical deposition process of lead (Pb) on the gold electrode surface and simultaneously measured ex-situ cyclic voltammogram. The utilized three-electrode electrochemical cell consists of a gold wire working electrode, counter electrode, reference electrode, and liquid electrolyte of 0.05M aqueous solution of $Pb(NO_3)_2$.

Lead (II) nitrate is very soluble in water at room temperature, dissolving according to

$$Pb(NO_3)_2\,(s) \rightarrow Pb^{2+}(aq) + 2NO_3^-\,(aq) \qquad 4.1.1$$

Applying sufficient voltage across electrochemical cell leads to plating on the cathode,

$$Pb^{2+} + 2e^- \rightarrow Pb(s) \qquad 4.1.2$$

This reaction is reversible, so an electrode can serve as a source or a sink for Pb^{2+}.

The figure 19-A shows images from three consecutive full cycles of lead dendrite growth and collapse on the working electrode. The figure 19-B shows the CV plot, which was measured simultaneously by a potentiostat/galvanostat (VersaSTAT4, Princeton Applied Research) with a scan rate of 50 mVs^{-1}, scan range from -1.1V to +1.1V.

(1) At frame 1, there was no electrochemical reaction was observed, that means that no obvious movement of Pb^{2+} on the interface of electrode and electrolyte.

(2) At frame 2, applied voltage varied to -0.5V and reaction from equation 4.1.2 was started. Pb^{2+} received electron from working electrode and become dendritic structure of Pb on the surface of the electrode. These Pb dendrite continue to grow rapidly from it's tip part.

(3) At frame 3, the Pb dendrite from frame 2 continuously received electron from liquid electrolyte and grew to be the maximum at -1.1 V. Appeared to be a tree-like dendritic structure and remained for that shape about 10s.

(4) At frame 4, the tree-like dendritic structure from frame 3 started to strip accompanying the reversal of sweeping direction of applied voltage. The dissolution occurred mainly from it's tip, but it had not disappeared completely.

(5) At frame 5, the applied potential was scanned back to it's initial value and collapse of Pb dendrite was completed. However, Pb crystalline from the dissolution was remaining in the liquid electrolyte.

Frame 6-10 and frame 11-15 had similar reaction mechanism and procedure with frame 1-5.

As the red arrow indicated in Fig.19-B, with each consecutive cycle the current peaks decreased, perhaps because the remnant from dendrite stripping process increased the resistance of electrolyte.

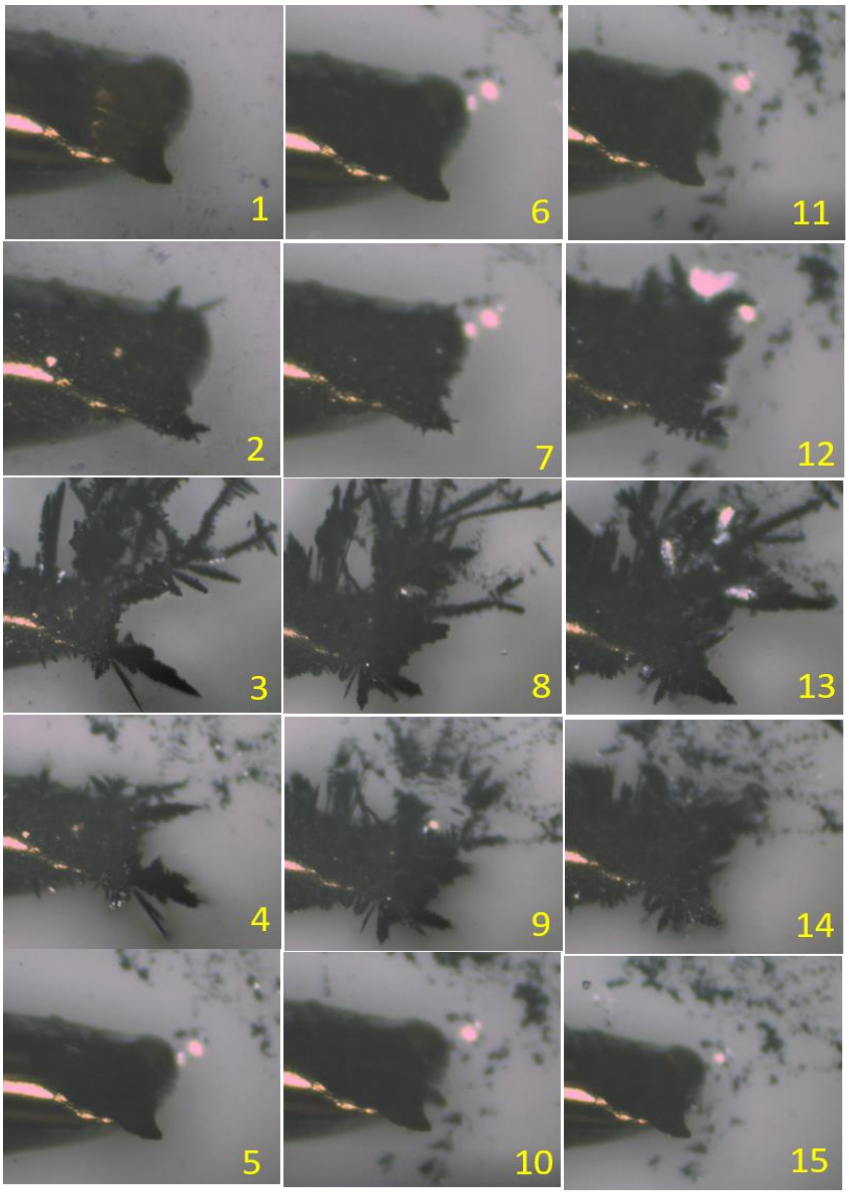

Fig. 19-A. Series of frames from three consecutive full cycles of optical microscope observation video of lead dendrite growth and collapse on a gold working electrode.

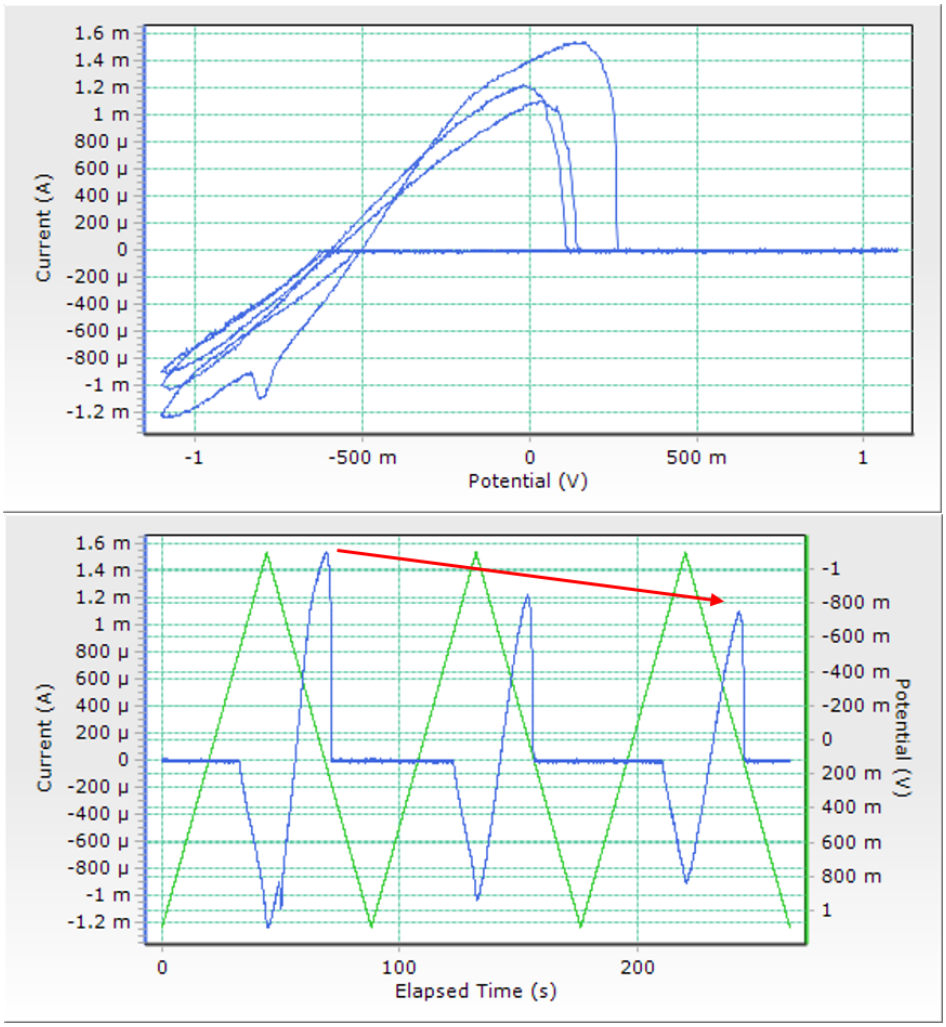

Fig. 19-B Ex-situ cyclic voltammogram. Cyclic voltammetry is performed at scan rate of 50 mVs^{-1}, scan range from -1.1V to +1.1V.

The cathodic current increases significantly at -0.5 V and this increase is accompanied by the formation of a noticeable Pb dendrite on the gold wire working electrode. Upon sweep reversal, the anodic current increases with a peak voltage around 0.2 V and the Pb dendrite is stripped.

Figure 20-A shows the lead dendrite growth and collapse on a gold electrode at the same experimental set with previous one, except for series of images were achieved from two different part of electrode and liquid electrolyte was 1.5M aqueous solution of $Pb(NO_3)_2$, also the scan range of applied voltage was from +1.3V to -1.3V.

Figure 20-A shows that the growth morphology of lead dendrite was different from previous experiment. In figure 19-A, the lead plating on the gold electrode was appeared to be tree-like dendritic structure. But this time it was more like blade-like structure and only grew from tip of the electrode (frame 6-15 from figure 19-A). In addition, the lead dendrite collapsed and disappeared completely throughout all three cycles and no obvious decrease of current peaks as appeared in previous experiment was observed (Figure 20-B).

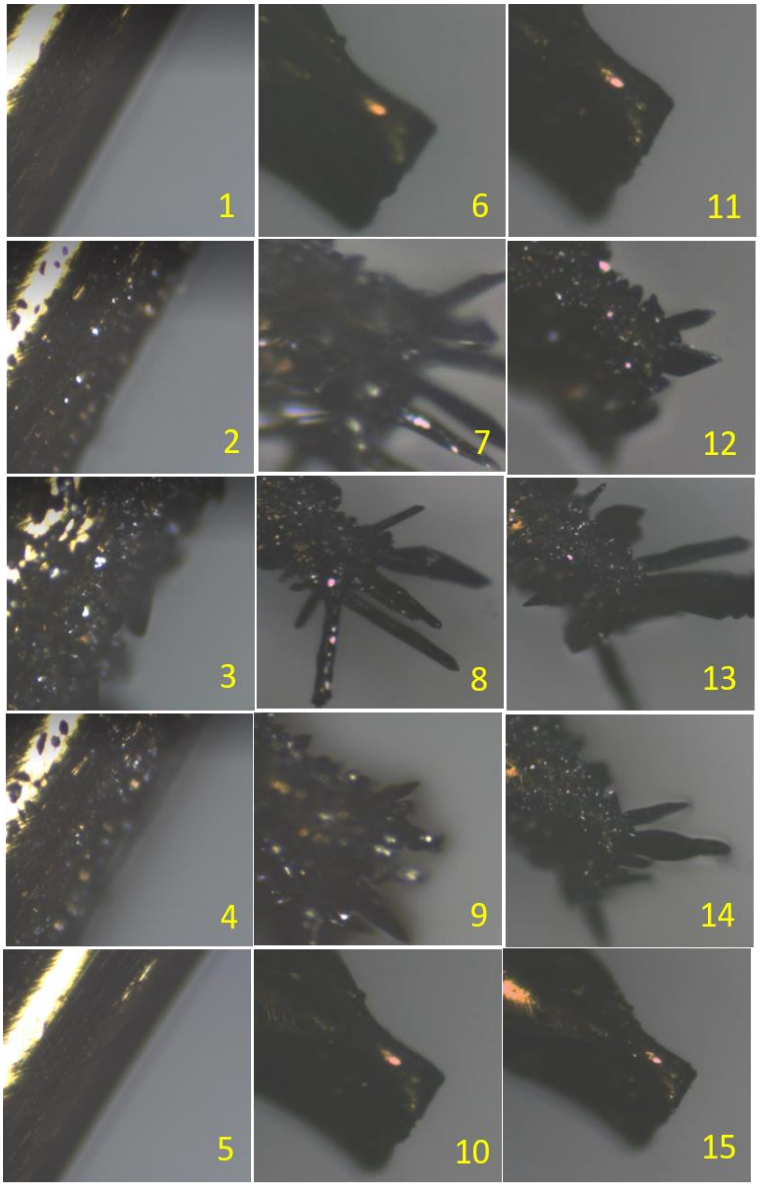

Fig. 20-A. Ex-situ cyclic voltammogram, Series of frames from three consecutive full cycles of optical microscope observation video of lead dendrite growth and collapse on a gold working electrode.

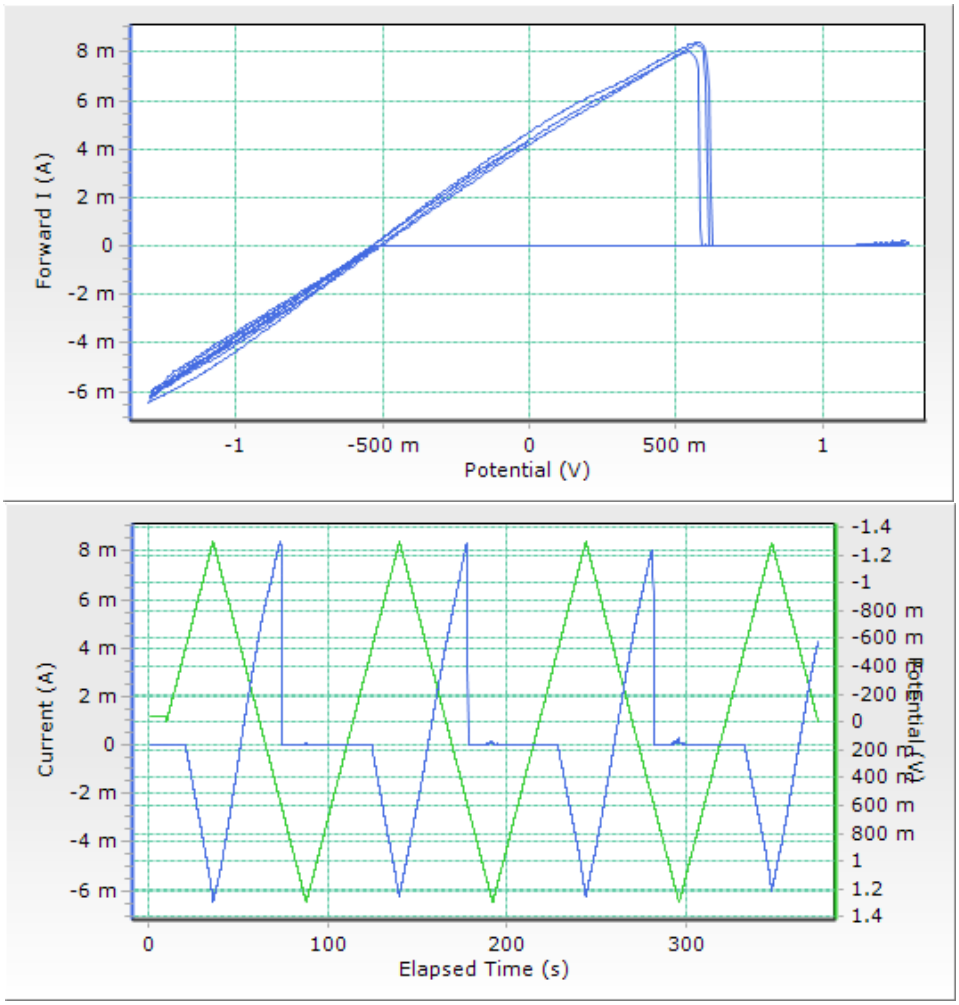

Fig. 20-B Ex-situ cyclic voltammogram. Cyclic voltammetry is performed at scan rate of 50 mVs^{-1}, scan range from -1.3V to +1.3V. The cathodic current increases significantly at -0.5 V and this increase is accompanied by the formation of a noticeable Pb dendrite on the gold wire working electrode. Upon sweep reversal, the anodic current increases with a peak voltage around 0.62 V and the Pb dendrite is stripped.

4.3 In-situ SEM observation

4.3.1 SEM observation of liquid specimen

Figure 21 shows the typical SEM images of Au nanoparticles of a diameter of ~10 nm (EM.GC10, BBI Solutions); (a) the particles were placed on the grid, faced to the vacuum side, and (b) the particles were placed on the back side of the grid, which were put into pure water filled in the cell. For the SEM image of [Fig. 21 (a)], the edge of the particles was clearly resolved, and the faint contrast of the particles were also imaged; those features seemed in agreement with the achievable resolution of the SEM. On the other hand, in Fig. 21 (b), the particles slightly looked blurred than those in Fig. 21 (a). Because of the electron window of the grid of a thickness of 50 nm, the passing electrons were scattered, leading to degradation of the spatial resolution of the SEM image. However, nanometer scale resolution of the SEM was able to be achieved still in water through the SiN membrane window of the grid, which worked well as a window in the vacuum of the SEM. Figure 15 shows the image of gold nanoparticles inside the water and in the vacuum. During in situ electron microscopy observation, most critical parts was the limited resolution of electron microscopy images inside liquid specimen compared to the usual

specimen. Even though the decrease of resolution of SEM image inside water compared to vacuum environment, it could be seen as the edges of gold nanoparticles was noticeable but getting blurry.

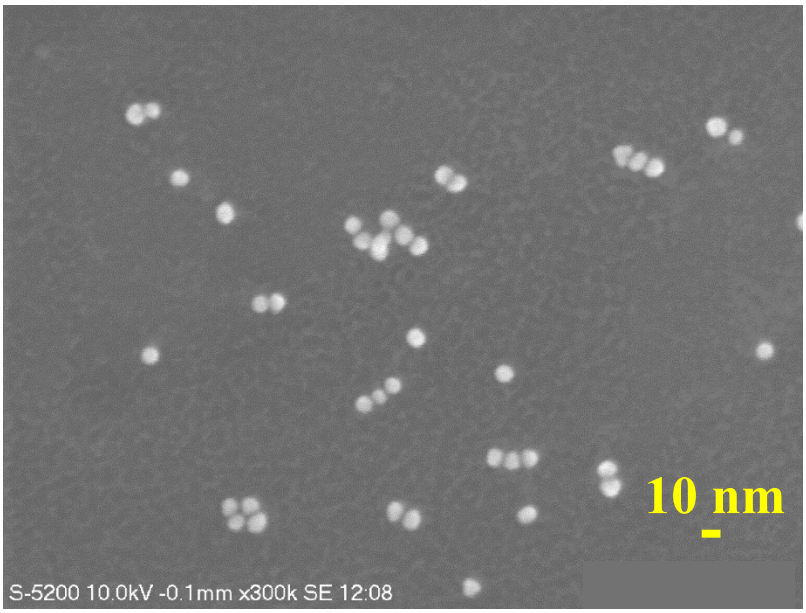

Fig. 21. SEM image of gold particles on the top of grid (in vacuum), and on the rear of grid (in water).

Also, the acceleration voltage of SEM might have negative effects on the electro-deposition and stripping of dendritic structure inside electrochemical cell. As well as it may cause secondary electron from the deposited metallic structure and lead too hard to distinguish the difference between applied voltage or acceleration voltage to the structure.

Figure 22 shows the cyclic voltommogram of in situ SEM observation of electro-plating and stripping of lead dendritic structure. As the emission current of 15 $\mu A \ \ and$ the acceleration voltage of SEM, 5 kV, 10 kV, 15 kV, 20 kV, 30 kV was used and 1.5 M $Pb(NO_3)_2$ as liquid electrolyte, sweep rate of 50 mV/s between range of $\pm 1.3\ V$

It shows that the different acceleration voltage of SEM has negligible effect on the current that caused following with the electro-deposition and stripping lead dendritic structure.

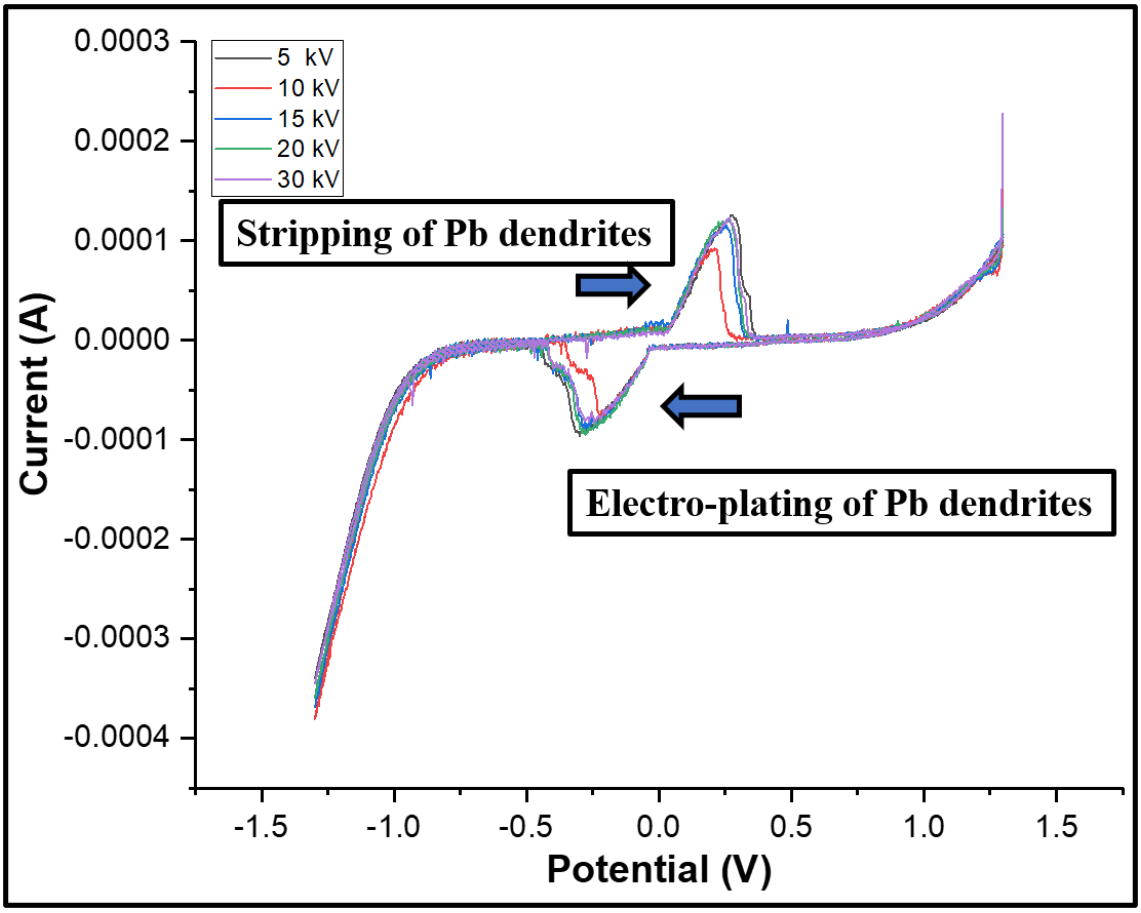

Fig. 22. In situ cyclic voltammogram under different SEM acceleration voltage of 5 kV, 10 kV, 15 kV, 20 kV, 30 kV, emission current 15 μA, sweep rate of 50 mV/s between range of $\pm 1.3\ V$, inside 1.5 M $Pb(NO_3)_2$ liquid electrolyte.

4.3.2 In situ SEM observation of electro-plating and stripping of lead dendrite

Figure 23 shows the visualization of the deposition and dissolution of Pb dendrites on the Au electrode in an electrolyte of 1 M $Pb(NO_3)_2$ via in-situ SEM observation. And the electrochemical reaction that caused the deposition and dissolution of lead dendrites could be expressed with following reaction

$$Pb^{2+} + 2e^- \leftrightharpoons Pb \qquad (1)$$

The bias voltage was swept at a rate of 50 mV/s in a triangular waveform in the range of $\pm 2\ V$ between the working and counter/reference electrodes.

First, no obvious change was observed in current and electrode-electrolyte interface when the bias voltage decreased from 2 V to 0 V; During this period, the energy of electrons inside electrode would increase and happen electron transfer with the lead ions from the liquid electrolyte around the electrode. At the point b, the concentration of lead ions around the electrode and the lead atoms that produced from electrochemical reaction would become equal. [1] From 0 V, small islands started to form at the electrode-electrolyte interface and turned into dendritic structures gradually, there was no obvious change to the measured current until the voltage reached –1.25 V. Then, electro-plating of lead

crystallization occurred at the interface of electrode-electrolyte interfaces; lead crystal islands formed uniformly surrounding the interface according to equation (1); blade-shaped dendritic structure grew from these islands and reached to its peak at point c. And the current increased rapidly because of electron transfer rate happened at the interface, also reached to its peak at the same time. The reduction rate increased continuously and reached to its peak at point c, lead ions from bulk solution would be carried to the interface by diffusion process.[1] During the process between point c and d, the lead dendritic structure stayed unchanged until the potential reached switching potential. the concentration of lead ions at the electrode surface would become almost 0 and the concentration of reduced lead atom at the electrode surface would reach highest level. The current decreased from peak current following the variation of reduction/oxidation agent in solvent. The diffusion layer would grow throughout the scan and inhibit the mass transport of lead ions to the electrode surface. It would slow down the rate of diffusion of lead ions from the bulk solution to electrode surface and resulting in a decrease in the current as the scan continues. [1] During the process between point d and e, lead dendritic structure would start to dissolve into liquid electrolyte rapidly as the reverse reaction of equation (1); and end of this process there would some lead dendrite

remnant left. The concentration of reduced lead atom at the electrode surface would decrease because of the oxidation and that of the lead ions at the electrode surface would increase; finally, these two become equal. The current increased since the increase of the rate of electron transfer happened during oxidation.[1] During the process between point e and f, lead dendritic structure would dissolve back to solvent. Start to dissolve from its tip and surface. Also, the currents increased simultaneously with stripping of lead dendritic structure. The concentration of reduced lead atom at the electrode surface would continue to decrease and that of the lead ions around the electrode surface would continue to increase and the rate of electron transfer reached highest level at point f.[1] During the process between point f and g, after the stripping process of lead dendritic structure completed, then the electrode surface change back to its original state, but the surface became more sharper and clearer visualized than before, it was due to the compensation of Pb crystallization on the Au electrode. The concentration of reduced lead atom at the electrode surface would reach lowest level and that of the lead ions around the electrode surface would back to the approximately original level as well as before electrochemical reaction.[1]

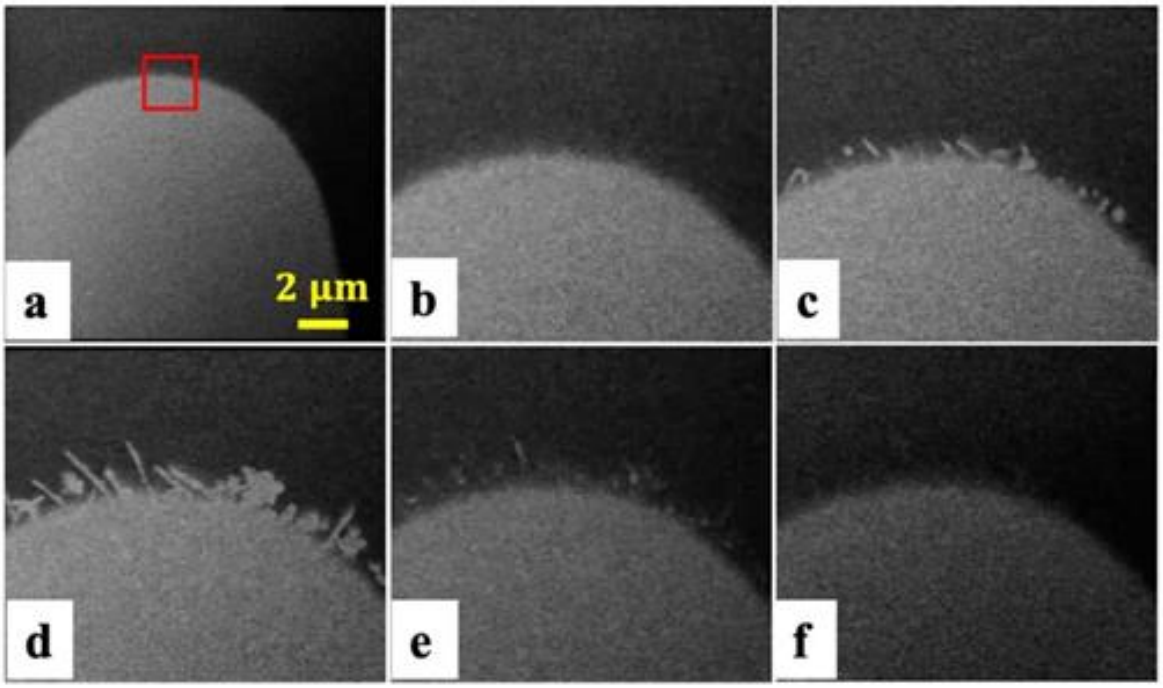

Fig. 23. Sequentially taken SEM images of electrochemical deposition and stripping of Pb on the Au electrode. The area denoted by the red square in the upper-left SEM image is zoomed in the SEM images in (a)–(e). Lower: applied voltage (in blue) and measured current (in orange) versus time. The moments indicated by points (a)–(e) correspond to the SEM images of (a)–(e), respectively.

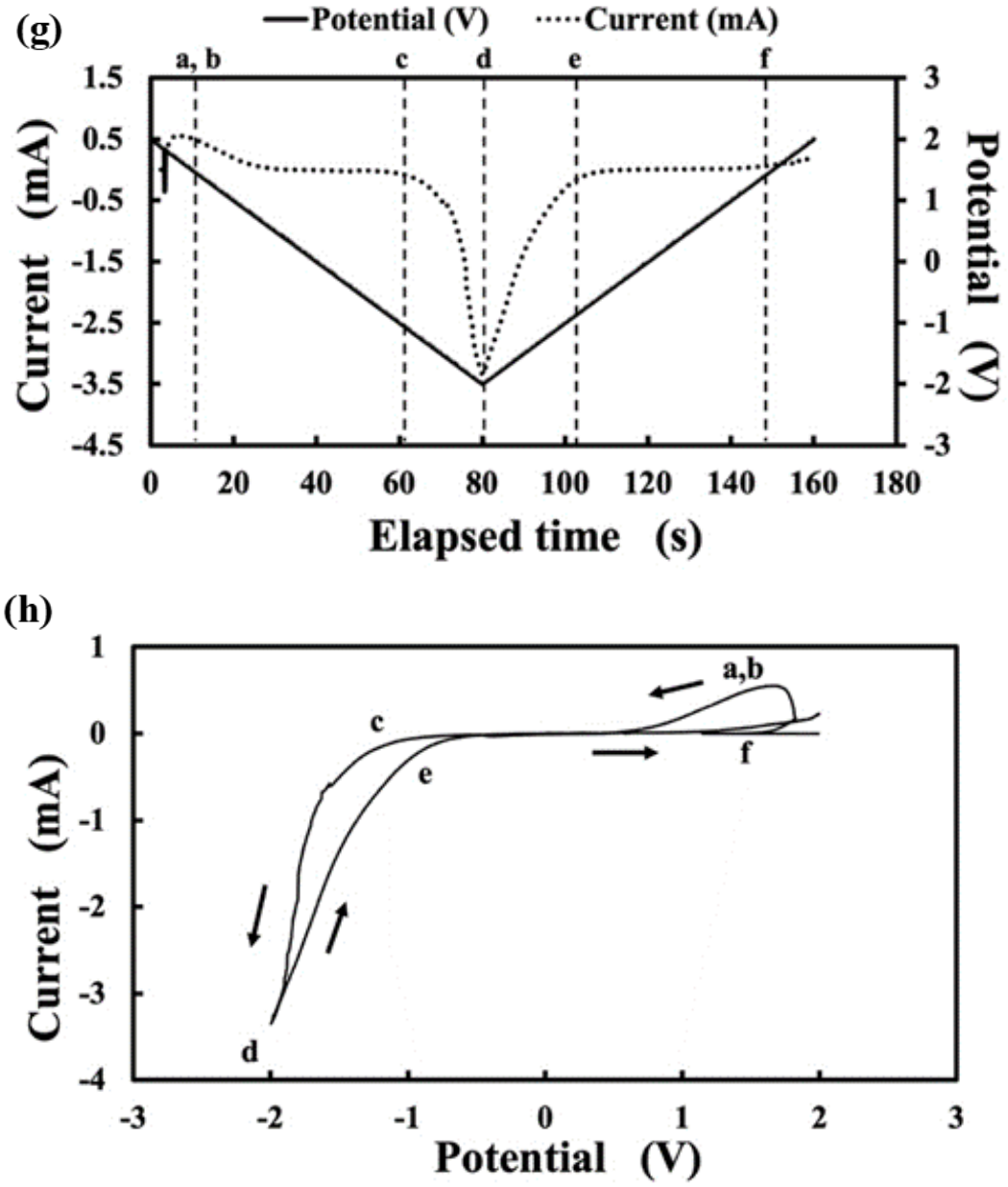

Fig. 24. Applied voltage (in blue) and measured current (in orange) versus time for Figure 23. The moments indicated by points (a)–(e) correspond to the SEM images of (a)–(e), respectively.

Similarly, Fig. 25 shows the results of the first cycle on the Au electrode with a smoother edge. At 2.0 V, no change was found as shown in Fig. 25(a) of the SEM image. As the potential was decreased, in Fig. 25(c) at 0.5 V, the edge of the Au electrode became brighter a little. In Fig. 25(d) at 0.0 V, particulate growth was noticeably observed at the edge of the Au electrode, whereas a white faint streak and small faint dots were also found slightly inside the electrode from its edge. In Fig. 25(e) at −0.5 V, the edge was abruptly decorated with the bright band, while the streak and dots grew partly. From Fig. 25(f) to (h) at −2.0 V, the dots looked to grow as dendrites, while the band structure also became thicker. Afterwards, the potential was changed reversely. In Fig. 25(j) at −1.1 V, the band structure was partly broken. From Fig. 25(j) to (k), the band structure was considerably diminished, and in Fig. 25(l) at −0.1 V, the band was reduced. On the other hand, the dendrite structures remained. In Fig. 25(m) at 0.3 V, the deposited band and dendrite structures almost disappeared; just before the peak current was detected at 0.1 V. The CV chart was shown in Fig. 26(r).

From the above results shown in Fig. 25, the peak current at −0.2 V (Fig. 26(r)) could be attributed to the electro-deposition of Pb mainly as the band structure, while the peak current passed at 0.2 V to the stripping of the Pb

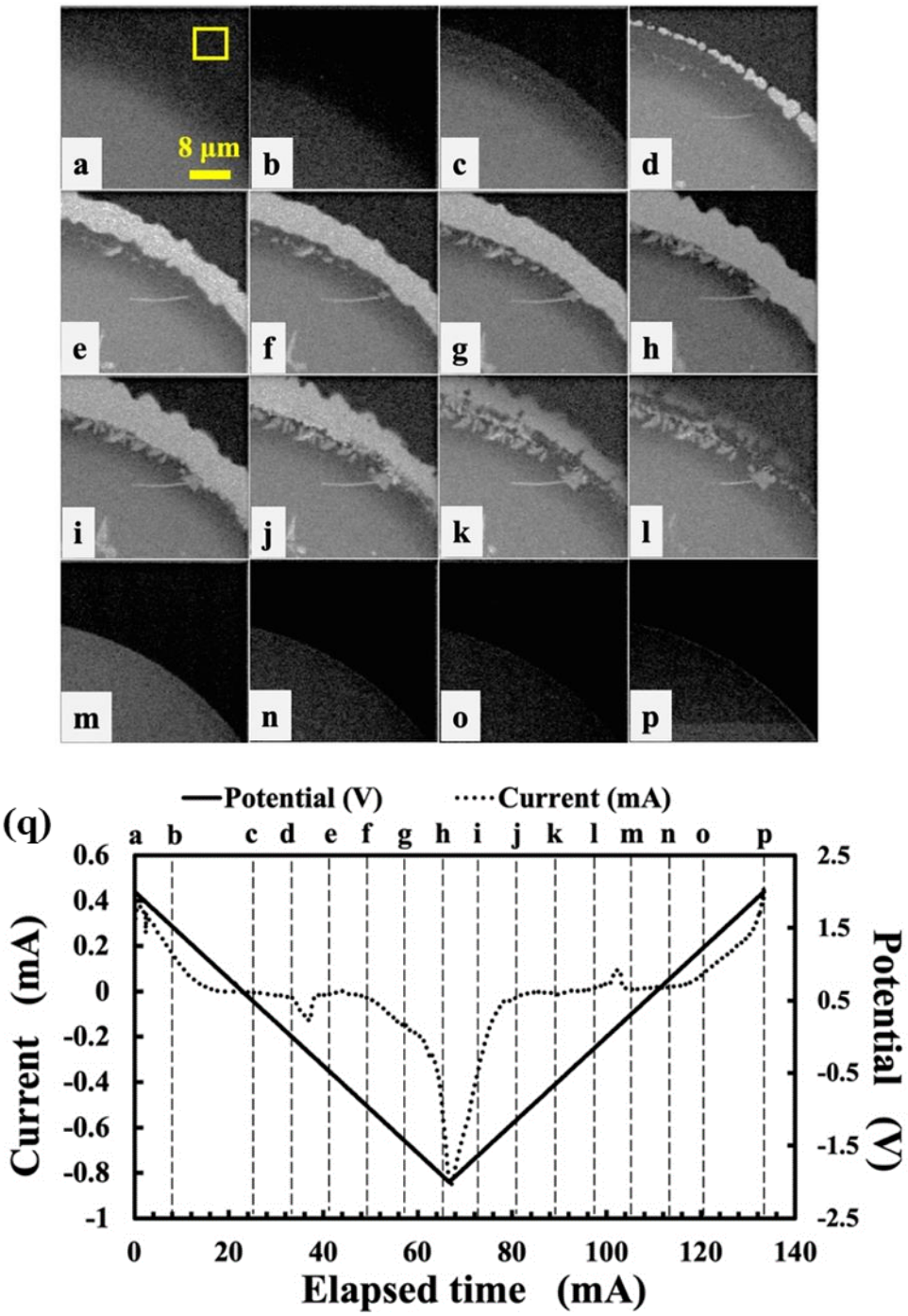

Fig. 25. (a)–(p) time lapse SEM images of the Au electrode with a smooth edge during the CV measurementn. (q) time evolution chart of the potential

and current of the CV simultaneously obtained with the SEM images in (a)–(p). The broken lines indicate the times when the respective SEM images were started to be taken for 8.4 sec.

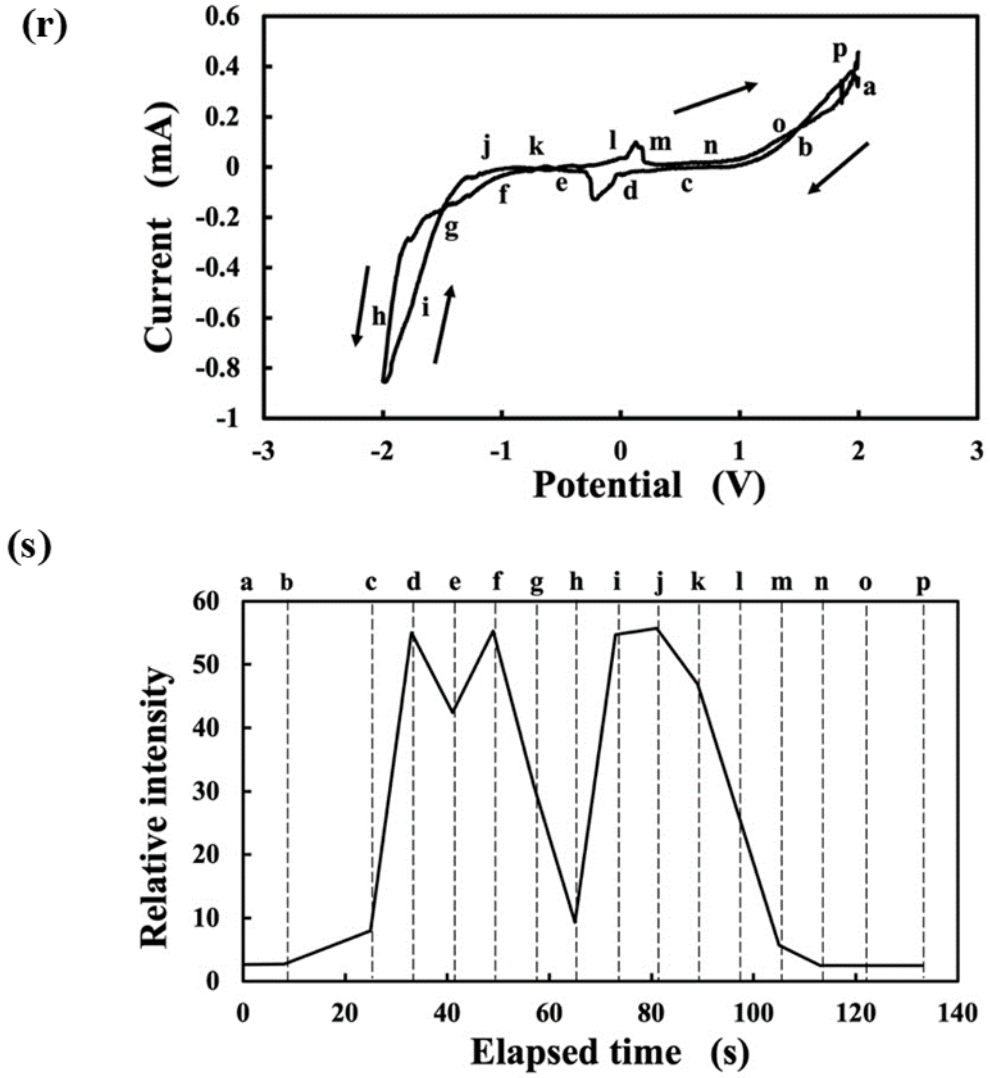

Fig. 26. (r) cyclic voltammogram plotted from (q). (s) Relative intensity change in the square region (denoted in yellow in (a)) in the SEM images from (a) to (p).

which were probably connected firmly to the Au electrode. On the other hand, it is probable the larger current between Fig. 25(f) and (j) was attributed to the growth of Pb over the Pb deposited regions and to the stripping from them. In Fig. 24, we did not observe the peak currents at ±0.2 V, and growth of the band structure. This indicates that the morphology of the Au electrode seriously affects the growth mode; the smooth edge promoted the band structure growth. In electrochemistry, the peak current at −0.2 V is regarded as underpotential deposition, meaning that the Pb layers were grown on the Au electrode. The rough edge of electrode perhaps suppressed the underpotential deposition. By applying higher negative potentials, the dendrites Pb growth was probably promoted at the specified sites even on the rough edge. This presented that the in-situ high-resolution SEM observation has high potential to distinguish the degrowth mode of electro-deposition and stripping by taking the correlation with the CV measurements.

Next, we also noticed the change in the brightness of SEM images during CV measurement, as shown in Fig. 26(s), in which the brightness of the region denoted by a square in Fig. 25(a) of the SEM image was plotted as a function of time. The brightness increased from (c) to (d) and decreased from (f) to (h), and, on the reversed potential change, increased from (h) to (i) and decreased

from (j) to (m). In general, the emissivity of secondary electrons is not simple but depends on the topographic shape and the applied potential as well as the atomic number Z of the sample.[30] Here, the topographic shape in the square region was the same, and the linear change in the potential did not produce the linear change in the brightness. Thus, we could assume that the brightness of the square region reflected the concentration of Pb with a higher Z number in the electrolyte. Thus, the followings would be extracted. From (a) to (c), a lot of Pb ions in the electrolyte moved to the counter electrode under the positive potentials applied to the working electrode. During the CV measurement with the varying potential, the Pb ions were collected closer to the working electrode. Then, the brightness was increased. Subsequently, the Pb ions were rapidly deposited on the working electrode and the Pb concentration was reduced in the square region. By reversing the potential, the Pb was stripped from the electrode and diffused around the electrode, resulted in the increase in brightness. Furthermore, the Pb ions moved to the counter electrode, and the Pb concentration was reduced. This scenario corresponded to the change of brightness in the square region of the SEM image. Although further study is required to clarify the mechanism, the application of in-situ SEM to electrochemistry sounds so promising.

Chapter 5. Conclusion

Understanding of the dendritic structure growth and stripping mechanism during electrochemical reactions is of great importance to improve the functionality of electrochemical technique devices. Thus, a lot of devoted works had been conducted to uncover the mechanisms qualitatively and quantitatively through combination of typical electrochemical measurements using macro scale electrodes. As an imaging technique during electrochemical reactions, electron microscopies with high resolution meet the desire for both the local structure of electrode and the dendrite formation at nanometer level characterization. For most of the previous works, transmission electron microscopy (TEM) was utilized for in-situ real time observation of metallic crystallization inside the liquid specimen. There have been difficulties like damages due to electron beam irradiation at thigh electric current densities and preparation of liquid specimen with thicknesses of thinner than 100 nm, which is the limitation of transmission of electrons in TEM, and so on. As for the in-situ pseudo real-time scanning electron microscopy (SEM) observation is more practical than TEM observation, because of relatively low current density and no particular requirement for the thickness of the specimen.

We developed a conventional in-situ electrochemical cell with two electrode terminals for SEM to observe the processes of electro-plating and stripping simultaneously with measuring the cyclic voltammetry. The cell was sized to fit into the small space of the custom-made specimen holder for Hitachi S-5200 Fe-SEM with several current feedthroughs, each of which was connected to a coaxial cable. The front plane of the cell-body possessed a drain on the side of an insulator plate with two holes for the cables, as well as a vessel for liquid electrolyte at the center of the insulator plate. The insulator had a circular depressed seat for a silicon nitrite TEM grid. Two Au wires inserted into Kapton tubes were connected to the two coaxial cables respectively, and inserted through the wire-holes of cell body and insulator; only the Au wires were set to the concentric hole and connected to two vapor-deposited Au electrodes on the one side of the TEM grid. There were two concentric circular seats for O-rings on a cell cover; one was smaller than the silicon nitrate grid and the other one was larger than that. Care was taken so as not for electrolyte to leak to the vacuum environment during SEM experiments. When the applied potential was varied, electrochemical reactions occurred at the end of the vapor-deposited electrode and were observed through a small thin silicon nitrite membrane

window of TEM grid with a thickness of 50 nm, through which the SEM electron beam was able to pass.

After inserting the SEM specimen holder assembled with the electrochemical cell into the SEM, the working electrode and the counter electrode of the two Au electrodes were electrically connected to the inputs of a potentiostat/galvanostat instrument (VersaSTAT4, Princeton Applied Research); the inputs for the counter and reference electrodes were connected each together for simple electrochemical measurements. We visualized the electro-plating and stripping of Pb dendrites on the Au electrode in an electrolyte of 1.5 M Pb(NO3)2 aqueous solution via in-situ SEM observation. The bias voltage was swept at a rate of 50 mV/s in a triangular waveform in the range from +2V to –2 V between the working and counter/reference electrodes. First, no obvious reaction was observed when the bias voltage decreased from 2 V to 0 V. From 0 V, small islands started to form at the electrode-electrolyte interface and turned into dendritic structures gradually, there was no obvious change to the measured current until the voltage reached –1.25 V. The dendritic structures rapidly grew with increasing current from –1.25 V, and the current peak appeared at –2 V. After the direction of sweeping voltage was reversed, the dendritic structures drastically dissolved with decreasing current up to –1.25

V. Afterward, the current showed no obvious change whereas the dendritic structure dissolved completely around 1.5 V. With increase in the sweeping rate, the peak value of the current and the redox potential difference increased. When the concentration and composition of electrolyte were changed, the reduction potential shifted toward the negative voltage direction and the oxidation potential shifted toward the positive direction. In-situ electron beam induced deposition was also observed and the mechanism was interpreted by the interaction between the Pb ion in the electrolyte and the secondary electron (SE) emitted from Pb particles.

In conclusion, our developed in-situ electrochemical cell for SEM observation fulfilled the needs for high resolution imaging and electrochemical measurement technique. The in-situ pseudo real-time SEM observation showed that the electro-plating and stripping of dendritic structure were consistent with the cyclic voltammogram curves. As the further work, development of the electrochemical cell with three electrodes and quantitively characterization of effect of electron beam irradiation during electron microscopy observation are required.

References

[1] N. Elgrishi, K. J. Rountree, B. D. McCarthy, E. S. Rountree, T. T. Eisenhart and J. L. Dempsey, J. Chem. Educ. 95(2), 197(2018).

[2] E. R. White, M. Mecklenburg, B. Shevitski, S. B. Singer, and B. C. Regan, Langmuir 28(8), 3695(2012)

[3] H. Ghassemi, M. Au, N. Chen, P. A. Heiden, and R. S. Yassara, Appl. Phys. Lett. **99**, 123113 (2011).

[4] R. L. Sacci, J. M. Black, N. Balke, N. J. Dudney, K. L. More, and R. R. Unocic, Nano Lett. 15(3), 2011(2015).

[5] M. J. Williamson, R. M. Tromp, P. M. Vereecken, R. Hull and F. M. Ross, Nature Mater 2, 532 (2003).

[6] N. d. Jonge, D. B. Peckys, G. J. Kremers and D. W. Piston, PNAS 106, 2159 (2009)

[7] M. Egawa, T. Ishida, L. Jalabert and H. Fujita, Appl. Phys. Lett. **108**, 023104-1 (2011).

[8] H. Zheng, R. K. Smith, Y. Jun, C. Kisielowski, U. Dahmen and A. P. Alivisatos, Science 324, 1309 (2009)

[9] J. E. Evans, K. L. Junggohann, N. D. Browning and I. Arslan, Nano Lett. 11, 2809(2011).

[10] N. M. Schneider, M. M. Norton, B. J. Mendel, J. M. Gorgan, F. M. Ross and H. H. Bau, J. Phys. Chem. C 118, 22373 (2014).

[11] A. Kushima, K. P. So, C. Su, P. Bai, N. Kuriyama, T. Maebashi, Y. Fujiwara, M. Z. Bazant and J. Li, Nano Energy 32, 271 (2017).

[12] M. Sun, H. G. Liao, K. Niu and H. Zheng, *Sci Rep* **3,** 3227 (2013).

[13] E. R. white, S. B. Singer, V. Augustyn, W. A. Hubbard, M. Mecklenburg, B. Dunn and B. V. Regan, ACS Nano 6(7), 6308(2012).

[14] Y. Oshima, T. Tsuda, S. Kuwabata, H. Yasuda, K. Takayanagi Y. Oshima et al., Microscopy 63, 481(2014).

[15] R. L. Sacci, N. J. Dudney, K. L. More, L. R. Parent, I. Arslan, N. D. Browning and R. R. Unocic, Chem. Commun. 50, 2104 (2014).

[16] E. Jenson, C. Købler, P. S. Jenson and K. Mølhave, Ultramicroscopy 129, 63 (2013).

[17] F. Orsini, A. D. Pasquier, B. Beaudouin, J. M. Tarascon, M. Trentin, N. Langenhuizen, E. D. Beer and P. Notten, Journal of Power Sources 76, 19 (1998).

[18] F. Orsini, A. D. Pasquier, B. Beaudouin, J. M. Tarascon, M. Trentin, N. Langenhuizen, E. D. Beer and P. Notten, Journal of Power Sources 81-82, 918 (1999).

[19] B. Sun, X.W. Zou and Z. Z. Jin, Material Science and Technology 20, 864 (2004),

[20] N. D. Nikolić, K. I. Popov, E. R. Ivanović, G. Branković, S. I. Stevanović and P. M. Živkovićb, Journal of Electroanalytical Chemistry 739, 137 (2015).

[21] B. Sun, Z. T. Yang, X. W. Zou and Z. Z. Jin, Materials Chemistry and Physics 86, 144 (2004).

[22] A. S. Kashin and V. P. Ananikov, Nature Rev. Chem. **3**, 624 (2019).

[23] W. Inami, K. Nakajima, A. Miyakawa, and Y. Kawata, Opt Express **18**,12897 (2010).

[24] N. de Jonge and F. M. Ross, Nature Nanotech. **6**, 695 (2011).

[25] J. E. Evans, K. L. Jungjohann, N. D. Browning, and I. Arslan, Nano Lett. **11**, 2809 (2011).

[26] K. L. Jungjohann, S. Bliznakov, P. W. Sutter, E. A. Stach, and E. A. Sutter, Nano Lett. **13**, 2964 (2013).

[27] H.-G. Liao, D. Zherebetskyy, H. Xin, C. Czarnik, P. Ercius, H. Elmlund, M. Pan, L.-W. Wang, and H. Zheng, Science **345**, 916 (2014).

[28] B. L. Mehdi, et al., Nano Lett. **15**, 2168 (2015).

[29] T. Tsuda, T. Kanetsuku, T. Sano, Y. Oshima, K. Ui, M. Yamagata, M. Ishikawa, and S. Kuwabata, Microscopy **64**, 159 (2015).

[30] G. Rong, X. Zhang, W. Zhao, Y. Qiu, M. Liu, F. Ye, Y. Xu, J. Chen, Y. Hou, W. Li, W. Duan, and Y. Zhang, Adv. Mater. **29**, 1606187 (2017).

[31] T. Tsuda, K. Hosoya, T. Sano, and S. Kuwabata, Electrochim. Acta **319**, 158 (2019).

[32] T. Foroozan, S. Sharifi-Asl, and R. Shahbazian-Yassar, J. Power Sources **461**, 228135 (2020).

[33] X.-Y. Yu, J. Vac. Sci. & Technol. A **38**, 040804 (2020).

[34] N. de Jonge, D. B. Peckys, G. J. Kremers, and D. W. Piston, Proc. Natl. Acad. Sci. USA **106**, 2159 (2009)

[35] H. Zeng, W.-I. Liang, H.-G. Liao, H. L. Xin, Y.-H. Chu, and H. Zheng, Nano Lett. **14**, 1745 (2014).

[36] C.-Y. Chen, T. Sano, T. Tsuda, K. Ui, Y. Oshima, M. Yamagata, M. Ishikawa, M. Haruta, T. Doi, M. Inaba, and S. Kuwabata, Sci. Rep. **6**, 36153 (2016).

[37] W. F. van Dorp and C. W. Hagen, J. Appl. Phys. **104**, 081301 (2008).

[38] M. Suga, H. Nishiyama, Y. Konyuba, S. Iwamatsu, Y. Watanabe, C. Yoshiura, T. Ueda, and C. Sato, Ultramicroscopy **111**, 1650 (2011).

[39] R. Møller Nielsen, S. Canepa, M. N. Yesibolati, C. P. Nielsen, H. Bruus, H. Sun, and K. Mølhave, Microscopy and Microanalysis **24**, 338 (2018).

[40] L. V. Kouwen, A. Botman and C. W. Hagen, Nano Lett. **9**, 2149 (2009)

[41] K. Seshadri, K. Froyd, A. N. Parikh and D. L. Allara, J. Phys. Chem. **100**, 15900 (1996).

[42] T. Djenizian, L. Santinacci and P. Schmuki, Appl. Phys. Lett. **78**, 2940 (2001).

[43] W. Inami, K. Nakajima, A. Miyakawa and Y. Kawata, Optics Express **18**, 12897 (2010).

[44] Y. Nawa, W. Inami, A. Chiba, A. Ono, A. Miyakawa, Y. Kawata, S. Lin and S. Terakawa, Optics Express **20**, 5629 (2012).

[45] K. Rykaczewski, W. B. White and A. G. Fedorov, J. Appl. Phys. **101**, 054307 (2007).

[46] S. J. Randolph, J. D. Fowlkee and P. D. Rack, J. Appl. Phys. **97**, 124312 (2005).

[47] S. J. Randolph, J. D. Fowlkee and P. D. Rack, Critical Reviews in Solid State and Materials Sciences **31**, 55 (2006).

[48] W. F. V. Drop and C. W. Hagen, J. Appl. Phys. **104**, 081301 (2008).

[49] E. R. white, M. Mecklenburg, S. B. Singer, S. Aloni and B. C. Regan, Appl. Phys. Express **4**, 055201(2011).

[50] Y. Matsuno, E. Okonogi, A. Yoshimura, M. Sato, C. Sato J. Japan Inst. Met. Mater. **81(4)**, 192 (2017).

[51] H. Nishiyama, M. Suga, T. Ogura, Y. Maruyama, M. Koizumi,K. Mio, S. Kitamura and C. Sato, Microscopy **44 (4)**, 262 (2014).

[52] M. Suga, H. Nishiyama, Y. Konyuba, Y. Watanabe, S. Iwamatsu and C. Sato, Microscopy **46 (4)**, 137 (2011)

[53] S. Watanabe, J. JSPE **77 (11)**, 1021 (2011).

Research Accomplishment

Published paper:

He, Gada; Oshima, Yoshifumi; Tomitori, Masahiko,
"In-situ high-resolution scanning electron microscopy observation of electro-deposition and stripping of lead in an electrochemical cell",
Japanese Journal of Applied Physics **60**, 035509-1–6 (2021).

Conference presentations:

1. 14th International conference on Atomically Controlled Surfaces, Interfaces and Nanostructures (ACSIN-14) Dates: October 21 – 25, 2018

Venue: Sendai International Center, Sendai, Japan

Oral presentation: In-situ scanning electron microscopy observation of electro-plating and stripping of lead dendrites in an electrochemical cell

2. The 66th Japan Society of Applied Physics Spring Meeting, 2019
Dates: March 9 – 12, 2019

Venue: Tokyo Institute of Technology, Ookayama Campus, Tokyo, Japan

Oral presentation: Electro-plating and stripping of lead dendrites observed by in-situ scanning electron microscopy with an electrochemical cell

3. The 80th Japan Society of Applied Physics Autumn Meeting, 2019
Dates: September 18 – 21, 2019

Venue: Sapporo Campus, Hokkaido University, Sapporo, Japan

Oral presentation: In-situ scanning electron microscopy observation of lead dendrites grown in an electrochemical cell

4. Annual Meeting of the Japan Society of Vacuum and Surface Science 2019
Dates: October 28 – 30, 2019

Venue: Tsukuba International Congress Center, Tsukuba, Japan

Oral presentation: In-situ scanning electron microscopy observation of electrode–electrolyte interfaces in an electrochemical cell